Crystallization behaviour and morphological features of LARC-CPI*

Joan T. Muellerleile†, Brian G. Risch, David E. Rodrigues and Garth L. Wilkes‡
Department of Chemical Engineering, Polymer Materials and Interfaces Laboratory, Virginia Polytechnic Institute and State University, Blacksburg, VA 24061, USA

and Dumont M. Jones
Tripos Associates, Inc., 1699 South Hanley Road, Suite 303, St. Louis, MO 63144, USA
(Received 13 May 1992; revised 13 July 1992)

This work describes the crystallization behaviour and morphological features of the semicrystalline polyimide known as LARC-CPI. The study considers several features affecting crystallization behaviour such as inherent viscosity, crystallization temperature, melt temperature and time in the melt. Crystallization kinetics data were analysed using an Avrami analysis in conjunction with differential scanning calorimetry. Complications encountered when evaluating the crystallization exotherm for this analysis are also discussed. Morphological features were investigated using several techniques, including scanning electron microscopy (SEM), transmission electron microscopy (TEM), wide-angle X-ray scattering (WAXS), and small-angle X-ray scattering (SAXS). A permanganic etching technique combined with SEM successfully revealed morphological detail further supported by TEM results. This technique is also used to estimate the isothermal linear crystalline growth rate, G. The SEM and TEM data lend support to the Avrami data obtained by crystallization kinetics. SAXS results reflect the influence of crystallization temperature on the long spacing. SAXS also reveals the presence of a broad second scattering peak for semicrystalline samples which appears in the same position regardless of crystallization temperature or inherent viscosity. Molecular modelling predicts a low-energy helical conformation with a near-periodic repeat distance corresponding to that of the second SAXS peak. The periodic character of this conformation is offered as a hypothesis for that peak. This work also considers the effect of potential nucleating agents on the recrystallizability of a higher inherent viscosity LARC-CPI. One of the several nucleators investigated appears effective in enhancing the bulk crystallization rate.

(Keywords: LARC-CPI; crystallization kinetics; crystallinity; morphology; molecular modelling; nucleating agents)

INTRODUCTION

Polyimides are becoming increasingly important in many industries. Some of the attractive general properties of these materials include high use temperature, good dimensional stability, chemical and thermal resistance, flame retardance with low smoke evolution, and good electrical properties. Improved properties and processability are undoubtedly expanding the importance of polyimides even further. As an example, aromatic polyimides in particular are being utilized in applications such as aerospace and electronic materials. Some of the advantages that this class of polyimides has to offer include even higher use temperatures, outstanding thermo-oxidative resistance, high tensile modulus, self-extinguishability if ignited, and reasonably low dielectric constants. As a consequence, these materials offer a lightweight alternative to inorganics and metals in high-performance applications such as aerospace and electronic materials[1–8].

Within the realm of aromatic polyimides, thermoplastics have received increasing attention in recent years. Although less information is available for thermoplastic polyimides than for their thermosetting counterparts, considerations such as processability and improved properties compared to thermosets have sparked greater research efforts in this area. Aerospace applications, for example, require materials that are able to withstand a wide range of performance conditions. Materials utilized for high-speed aircraft can be subjected to temperatures of 260°C and above for thousands of hours, while those used for missiles may require temperatures in the range of 540°C and higher for tens of seconds. To this end, a portion of ongoing research at NASA-Langley Research Center has been dedicated to developing thermoplastic aromatic polyimides for high-performance applications such as structural adhesives and composites[4–6].

Although polyimides utilized for most applications are typically amorphous, the importance of crystallinity has led to recent efforts to develop semicrystalline polyimides which are also suitable. Cheng and co-workers have recently reported on the crystallization kinetics and

* Presented at 'Advances in Polymeric Matrix Composites', 5–10 April 1992, San Francisco, CA, USA
† Current address: Monsanto Company, 700 Chesterfield Village Parkway, St. Louis, MO 63198, USA
‡ To whom correspondence should be addressed

0032-3861/93/040789-18
© 1993 Butterworth-Heinemann Ltd.

morphological features of a semicrystalline polyimide containing 4,4′-oxydiphthalic anhydride (ODPA) and varied lengths of ethylene glycol[2,9,10]. However, limited data of this nature for more rigid chain polymer systems in general suggests that such information would be desirable. Indeed, having the ability to maintain the appropriate level and type of crystallinity is a crucial consideration for these materials, since crystallinity can critically affect properties such as stiffness, solvent and environmental resistance, and use at temperatures above the glass transition temperature, T_g. Another important point is that the apparent crystallization window, ΔT_a, is ~130°C. This window is defined as $T_m - T_g$, where T_m is the observed melting point (as opposed to the equilibrium melting point T_m^0). This window is not large, especially compared to other semicrystalline thermoplastics such as poly(aryl ether ether ketone) (PEEK) or poly(phenylene sulphide) (PPS), which have apparent crystallization windows of ~190 and 200°C, respectively. The issue of the crystallization window will be addressed later in this work. Additionally, the thermal process used to imidize LARC-CPI (as opposed to solution or chemical imidization) induces crystallization during imidization. However, recrystallization also develops following melting of the imidized film, but little work has been undertaken to investigate the process by which the respective morphologies develop. This issue of recrystallization following melting suggests that one of the most important variables affecting crystallization is processing (or thermal) history[11–22]. In addition to isothermal crystallization temperature and times mentioned in conjunction with crystallization kinetics, processing history includes other considerations such as time and temperature in the melt[11,12,15,17,19,23,24]. Time and temperature in the melt will generally affect the number of nucleation sites remaining in the material[11,12,15,17,19,24]. As the temperature increases, more nuclei will be destroyed[11,14,24]. Increased holding time in the melt can have a similar effect[11,15,17,19]. Furthermore, if insufficient melting occurs, residual nuclei will promote more rapid bulk crystallization with cooling[12,23]. The dependence of the number of surviving nuclei on time and temperature in the melt is frequently observed for semicrystalline thermoplastics[19]. This dependence also appears to be stronger for polar *versus* non-polar polymers[25–28]. The final semicrystalline superstructure (such as spherulitic, for example) size is a function of the melt temperature and time in the melt through the nucleation density[23,24]. This decrease in nucleation density leads to a lower bulk crystallization rate as well as the formation of larger superstructures. The size of the superstructure has been shown to affect mechanical properties such as failure behaviour and impact strength, where an increase in size results in a decrease in these properties[23,24]. The importance of thermal history prior to crystallization cannot therefore be overlooked. Furthermore, the crystallization rate may possibly be affected by factors such as nucleating agents. Nucleating agents are often employed as a means of increasing the crystallization rate through providing additional nucleating sites. Nucleating agents are frequently used to seed polymer melts or solutions, and can vary the size, number, type and rate of formation of developing semicrystalline superstructures within the material[11,12,29]. This can, in turn, affect material properties including optical properties such as enhanced transparency, and mechanical properties such as impact resistance, tensile strength and elongation at break, as well as optimizing processing time[30,31]. Thus, in order to most effectively utilize the advantages offered by the presence of crystallinity, it is first necessary to gain an understanding of the material's crystallization behaviour and morphology.

A semicrystalline aromatic polyimide originally developed at NASA-Langley constitutes the focus of this work, namely LARC-CPI (Langley Research Center Crystalline Polyimide)[4–6]. The thermal, mechanical and adhesive properties reported for this material are sufficiently outstanding to merit further investigation of the structural features of this system and promote further understanding of its crystallization behaviour[4–7,32]. The purpose of this present report is to provide this information and to account for the influence of specific variables on morphological behaviour. These variables include molecular weight (as indicated by inherent viscosity of the precursor poly(amic acid)), crystallization temperature, melt temperature, melt time and nucleating agents. Results from several characterization techniques and analyses which assess the effect of these features are presented as a means of beginning to elucidate the crystallization and morphological features of LARC-CPI.

EXPERIMENTAL

Materials

All LARC-CPI materials and nucleating agents utilized for this study were synthesized and provided by NASA-Langley. The chemical structural repeat unit of LARC-CPI is shown in *Figure 1*. It is noted that the repeat unit is quite large and has a molecular weight of 787. The polyimides were synthesized, then imidized using the stepwise bulk thermal imidization procedure described in an earlier publication[33]. Briefly reviewed, films were imidized by casting the precursor poly(amic acid)s onto plate glass and curing for 1 h each at 100, 200 and 300°C. Sample designations and inherent viscosities for the precursor poly(amic acid)s, for the as-received (or as-cast) four principal films discussed in this work are listed in *Table 1*. A potential note of caution in conjunction with the values in *Table 1* is that the actual molecular weight distribution is unknown. While it would be anticipated that this polydispersity of the

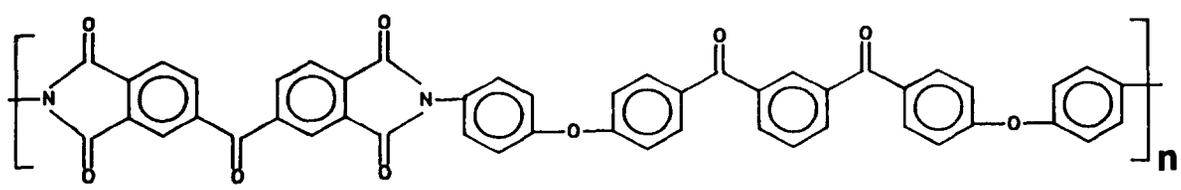

Figure 1 Chemical structural repeat unit of LARC-CPI

Table 1 Sample designations and inherent viscosities of LARC-CPI films

Sample designation	Inherent viscosity, η_{inh} ($dl\,g^{-1}$)[a]
CPI-0.69	0.69
CPI-1.05	1.05
CPI-1.24	1.24
CPI-1.49	1.49

[a] Poly(amic acid) determined at a concentration of 0.5% in DMAc at 25°C

distribution might be approximately 2 (because the polymerization is step-growth) it is likely to be broader since the stoichiometry is not balanced for purposes of varying the molecular weight, as discussed elsewhere[34]. No experimental data on the polyimide molecular weight are available at this time because of difficulties encountered in finding a suitable solvent system for the fully-imidized material. All polyimides listed in *Table 1* were end-capped with aniline. Much of the adhesive, composite and solvent resistance work which was previously discussed was conducted by NASA researchers on end-capped LARC-CPI, where phthalic anhydride was the end-cap. A study by Hergenrother *et al.* evaluating the effect of different end-caps on thermal behaviour and other properties reported that the aniline end-capped LARC-CPI showed superior melt flow and comparable thermo-oxidative stability compared to the phthalic anhydride end-capped CPI[34]. The effect of thermal stability on crystallization behaviour will be addressed later in this work. The imidized films used for this work were transparent and amber in colour, having a thickness of ~25–50 μm.

Techniques

The as-received LARC-CPI films were subjected to further thermal treatment by melting at either 375 or 385°C, then recrystallizing at various temperatures in preheated aluminium blocks, as described in previous reports[33,35]. The amorphous nature of the film following melting at these elevated temperatures was verified by differential scanning calorimetry (d.s.c.) and wide-angle X-ray scattering (WAXS). The as-cast films had different 'surfaces' as a consequence of being cast onto plate glass prior to the imidization process. These surfaces will be designated as air and glass, respectively. When recrystallized in the thermal chamber, however, the samples were suspended in a test tube which was then placed inside the aluminium block. The original as-cast surfaces were therefore both subjected to air during the recrystallization process. Results presented here are for films of different inherent viscosities recrystallized at various temperatures.

D.s.c. was performed using either a Perkin-Elmer DSC-4 or a Seiko model 210. The Perkin-Elmer calorimeter was calibrated using an indium standard scanned at 10°C min^{-1}. Higher temperature accuracy was checked using tin and zinc standards. The Seiko calorimeter was calibrated with indium, tin and zinc standards.

Samples were prepared by weighing them in aluminium pans using a Mettler AE 160 balance to an accuracy of 0.1 mg. Sample sizes were typically ~10 mg and 5 mg when using the Perkin-Elmer and Seiko, respectively. Variation in sample weights was limited to ±0.1 mg whenever possible. Samples were run under nitrogen at a purge pressure of 138 kPa in the Perkin-Elmer and 345–690 kPa in the Seiko. A scanning rate of 20°C min^{-1} was utilized unless otherwise noted.

Isothermal crystallization kinetics were carried out in the Perkin-Elmer. Samples were heated at a rate of ~50°C min^{-1} to either 375°C or 385°C and melted for 2 min. They were then quenched at a rate of ~200°C min^{-1} to the desired crystallization temperature and allowed to remain at that temperature until little variance in the baseline was observed. This baseline (or heat flow rate) invariance following the exotherm was used to approximate the completion of the crystallization process detectable by d.s.c. at that temperature. Samples were then typically scanned directly from the crystallization temperature to 400°C at 20°C min^{-1} to determine heat of melting and melting temperature values as a function of crystallization temperature.

Scanning electron microscopy (SEM) and transmission electron microscopy (TEM) were carried out as previously described[33]. Structural detail in CPI samples prepared for SEM has been successfully revealed by utilizing the permanganic etching technique of Olley and co-workers for PEEK. The details of this etching procedure are described elsewhere[33,36].

A STOE Bragg–Brenatto-type transmission X-ray diffractometer was used for angular WAXS measurements. Copper K_α radiation was used as the radiation source, with graphite as the monochromator. The operating conditions were 40 kV and 20 mA. The goniometer was calibrated with a silicon standard. Constant time measurements of 20–60 s (depending upon sample thickness) were made at 2θ intervals of 0.1°. Samples were scanned through an angular range of 10–35°. The film specimens were mounted in a flat film holder. Samples were rotated at a constant rate during scanning to eliminate possible orientational effects resulting from the casting process. No signs of orientation existed using a flat plate Warhus camera; however, this did not preclude possible equal in-plane orientation, as will be discussed later. The data in the present work were analysed using the Siemens Polycrystalline Software package.

Small-angle X-ray scattering (SAXS) measurements were made using a Siemens Kratky camera system with a 50M Braun position-sensitive detector from Innovative Technology, Inc. A Phillips model PW 1729 tabletop generator was used. Operating conditions were 40 kV and 20 mA. The radiation source was nickel-filtered copper K_α. Lead stearate was used as a calibration standard for the scattering angle. Lupolen® polyethylene was utilized for absolute intensity measurements. A computer program developed by Vonk was used to desmear the data[37].

Computer modelling involved molecular dynamics and repeated conformational minimization of a series of structural repeat units. More detail describing the procedures utilized will be presented in the Results and Discussion section.

Preparation of nucleated LARC-CPI films

A 15% w/w poly(amic acid) solution end-capped with aniline having an inherent viscosity of 1.24 $dl\,g^{-1}$ was used to prepare LARC-CPI films containing nucleating agents. The end-capped poly(amic acid) was selected in order to help prevent side reactions during imidization. The solution was utilized as-received from NASA.

Several potential nucleators were investigated, including a very low-inherent-viscosity LARC-CPI powder and three low-molecular-weight compounds whose structures are related to that of LARC-CPI. Chemical structures and nomenclature for these four nucleating agents are listed in *Table 2*. The imidized low inherent-viscosity CPI powder was end-capped, but with phthalic anhydride instead of aniline. The inherent viscosity for this polyimide was 0.38 dl g^{-1} as determined at 0.5 wt% concentration in 60/40 *o*-chlorophenol/phenol at 25°C. The inherent viscosity of the precursor poly(amic acid) was 0.4 dl g^{-1} as determined at 0.5 wt% concentration in dimethylacetamide (DMAc) at 25°C[38]. The three low molecular-weight nucleators given in *Table 2* were also end-capped with phthalic anhydride to help prevent side reactions potentially leading to, for example, a reduction in the molecular weight of the original high-inherent-viscosity poly(amic acid). Melting points for the four potential nucleating agents are also listed in *Table 2*. The high values of these temperatures combined with the rapid crystallizability of the materials led to their selection, although further rationale for these choices will be provided later.

A high level (5 wt%) of each nucleating agent was added to the 15% w/w poly(amic acid) solution described earlier. As the poly(amic acid) was already dissolved in DMAc, the DMAc was chosen as the solvent for the nucleating agents. As the low-inherent-viscosity CPI powder, however, was already imidized, it did not dissolve in DMAc. It was therefore added directly to the poly(amic acid) solution. (Had the amic acid form been available, it would have dissolved well at room temperature.) The other three low-molecular-weight nucleators were first dissolved in DMAc to evaluate solubility. PDA-PA dissolved in DMAc at elevated temperatures in the range of 160°C but precipitated out of solution below 130°C. There was concern regarding possible inducement of some imidization prior to the actual thermal imidization process if the heated PDA-PA/DMAc solution were added to the poly(amic acid). As a consequence, the PDA-PA powder was added directly to the poly(amic acid). The remaining low-molecular-weight nucleators dissolved in DMAc at room temperature, so these were dissolved in DMAc prior to addition to the poly(amic acid) solution. Each nucleating agent was stirred into the poly(amic acid) and cast as a thin film with a wet thickness of 250 μm on a Pyrex glass plate using a doctor blade. A control film without nucleating agent was also cast. Films were allowed to dry overnight at ambient temperature and pressure in a vacuum oven equipped with a slow dry air purge. The air was dried by first passing it through a column filled with silica gel. The tack-free films were then imidized in a Blue M circulating air oven for 1 h at 100°C, then heated to 200°C and held at that temperature for 1 h. They were immediately transferred to a Pasadena Hydraulics film press preheated to 200°C, and then heated to 300°C. The thermal treatment outlined here was designed to mimic that utilized at NASA-Langley as closely as possible. A Blue M oven was not used for the entire process because of upper temperature limitations of the oven. Following the final stage of imidization of 1 h at 300°C, the films were allowed to cool slowly in the press to ambient temperature. The final films of ~25–50 μm were removed by immersing the plates in hot water and, if necessary, stripping the film off the glass. Referring to the designations in *Tables 1* and *2*, these films are denoted as FC-CPI-1.24 (CPI-0.40), FC-CPI-1.24 (PDA-PA), FC-CPI-1.24 (3,4′ DABP-PA), and FC-CPI-1.24 (4,4′ DABP-PA). The designation of FC refers to a film cast in our laboratory using a precursor poly(amic acid) supplied by NASA-Langley. This poly(amic acid) was the same solution from which the NASA researchers cast the film designated in *Table 1* as CPI-1.24. The listings in parentheses refer to the potential nucleating agents listed in *Table 2*.

Table 2 Sample designations, chemical structures and melting points for potential LARC-CPI nucleating agents

Designation	Chemical structure	T_m (°C)
CPI-0.40	CPI repeat unit end-capped with phthalic anhydride	359
PDA-PA[a]	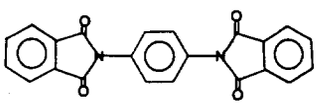	374
3,4′ DABP-PA[b]	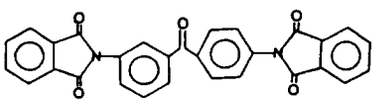	289
4,4′ DABP-PA[c]	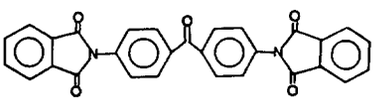	299

[a] PDA-PA = phenylene diamine end-capped with phthalic anhydride
[b] 3,4′DABP-PA = 3,4′-diaminobenzophenone end-capped with phthalic anhydride
[c] 4,4′DABP-PA = 4,4′-diaminobenzophenone end-capped with phthalic anhydride

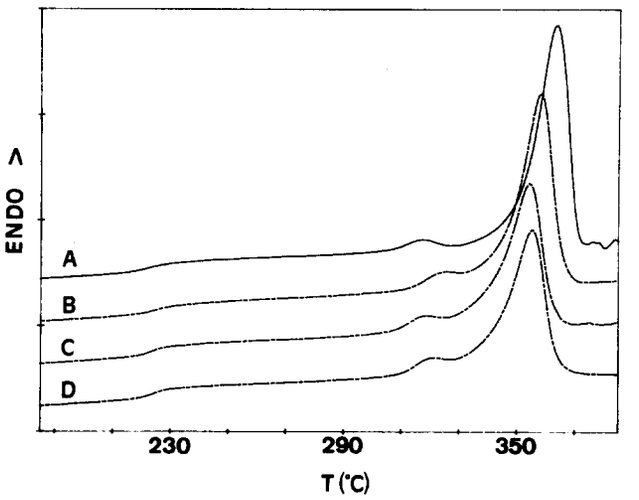

Figure 2 D.s.c. scans of as-received LARC-CPI films: A, CPI-0.69; B, CPI-1.05; C, CPI-1.24; D, CPI-1.49

RESULTS AND DISCUSSION

D.s.c. response of as-received (as-cast) LARC-CPI

D.s.c. scans for the as-received LARC-CPI films are shown in *Figure 2*. Scans A–D are for the lowest to highest inherent viscosities, respectively. With the exception of a slightly higher melting maximum for scan A, and a somewhat higher heat of melting with decreasing inherent viscosity, there appear to be no major differences between these first thermal scans. The small endotherm appearing

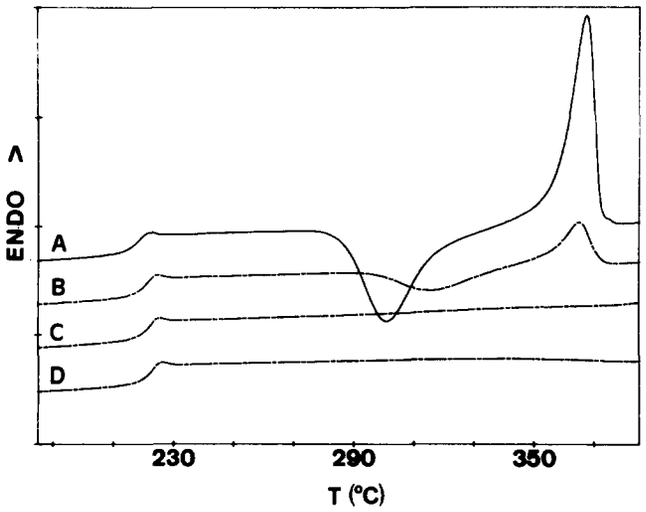

Figure 3 Second d.s.c. scans of as-received LARC-CPI films following an initial scan and quench; A, CPI-0.69; B, CPI-1.05; C, CPI-1.24; D, CPI-1.49

in the range of ~310–330°C results from the melting of smaller and less perfect crystals formed during the last stage of imidization at 300°C. This small endotherm, commonly observed in thermally treated semicrystalline polymers, is generally expected a little above (~20°C) the final annealing temperature[12]. The samples were scanned a second time after quenching, and results are shown in *Figure 3*. Once the imidization thermal history is erased, these second scans show an effect of inherent viscosity on recrystallization under these conditions. Referring to *Figure 3*, where scans A–D represent the lowest to highest inherent viscosity samples, respectively, it is clear that A and B show evidence of recrystallization while C and D do not. Furthermore, the heat of melting value for A is about four times larger than that obtained for B under these scanning conditions. Using inherent viscosity as an indication of molecular weight, it would be anticipated that the lowest inherent viscosity samples would recrystallize most readily and over the widest temperature range under these conditions, as was shown by Magill for poly(tetra methyl-*p*-phenylene)-siloxane[39]. Because the lowest inherent viscosity sample recrystallizes more readily than the other samples, it was utilized to examine effects of different melt temperatures and different times in the melt on recrystallization. These results will be presented subsequently. Another noteworthy point is the significant (~7°C) increase in the melting point maximum for the sample CPI-1.05 (scan B in *Figures 2* and *3*). The initial melting point may have been lowered because of a slightly lower crystallization temperature in the vicinity of 300°C during imidization. It is also noteworthy that the heat of melting value is not very high. At present, two possibilities could account for this: either there were low levels of crystallinity in the samples, or the heat of fusion for a fully crystalline sample is low. This issue will be considered later.

LARC-CPI crystallization kinetics

Evaluation of the crystallization exotherm. For the Avrami analysis, determination of the normalized crystallization content, $X_c(t)$, as a function of time required the evaluation of the crystallization exotherm. For the range of inherent viscosities investigated here, all of the aniline end-capped CPI materials recrystallized readily enough from the melt to use this method. However, the crystallization temperature, T_c, ranges examined varied somewhat as a function of inherent viscosity, i.e. 300–315°C for CPI-1.49 *versus* 330–345°C for CPI-0.69. This is a consequence of the fact that the higher inherent viscosity samples did not recrystallize rapidly enough at the higher temperatures and the lower inherent viscosity samples recrystallized too quickly at the lower temperatures to allow for the development of a crystallization exotherm suitable for analysis.

A complicating feature in the evaluation of $X_c(t)$ for the LARC-CPIs was the determination of the crystallization exotherm endpoints. Irrespective of inherent viscosity or T_c, all samples either began to crystallize immediately upon reaching T_c, or did not crystallize quickly enough to yield a detectable crystallization exotherm by d.s.c. in a reasonable time-frame to gather useful data. This is rather suprising, as it was anticipated that a wide enough range in T_c and inherent viscosities was covered such that the onset of crystallization would have been delayed, at least to some degree, with increasing temperature and inherent viscosity. It is not fully understood why this initial starting point of the crystallization exotherm consistently appeared immediately upon reaching the T_c. Part of the problem may well be related to insufficient time in the melt to erase existing nuclei, and this topic will be discussed later.

A second complication encountered was that the portion of the scan that developed following the exotherm, which served as part of the baseline, was typically lower in height than the starting point of the crystallization exotherm. This baseline lowering may be a result of secondary crystallization of initially rejected material or due to changes in crystal perfection. In these cases, crystallization is known to occur at a considerably slower rate[12]. If the rate of the secondary processes is sufficiently slow relative to the time scale of the experiment, incremental increases in the baseline following the bulk of the crystallization may not be readily detected. It is not known whether this explanation does, in fact, account for the lowered baseline, or if the lack of change in the crystallization onset point is also a factor. A consistent trend in change of baseline lowering as a function of T_c and/or inherent viscosity was unfortunately not observed; if it had been, it might well have helped clarify this issue.

Because of the problems involved with the onset point of crystallization and lowered baseline following the exotherm, there was some question as to how the endpoint of the crystallization exotherm should be defined. Two approaches were investigated. The first used the onset of crystallization as the starting point and fixed the endpoint by equating the heat of crystallization to the heat of melting. The second method utilized the baseline following the exotherm as the endpoint and set the starting point by extending the baseline across the exotherm. The location of the exotherm starting point is arbitrarily defined by the baseline location. However, the authors do not believe that the apparent onset point, which appears immediately upon reaching T_c irrespective of inherent viscosity or choice of T_c, is necessarily any more valid. Furthermore, the baseline following the crystallization exotherm was typically consistently stable. This is regarded as lending more credence to the use of the baseline in defining the exotherm limits rather than using the apparent onset point of crystallization. In view

of the baseline extension method selected, an attempt will be made to note its effect on the Avrami parameters.

Effect of exotherm evaluation on Avrami parameters k *and* n. The investigation of different methods to evaluate the crystallization exotherm included assessing the effect of exotherm endpoint choice on the conventional Avrami parameters k (bulk crystallization constant) and n (the Avrami exponent). A brief study revealed that the value of k is quite sensitive to the endpoint variations such that a small change in the initial endpoint (starting point of exotherm) altered k significantly. As a consequence, k values will not be presented here. A variation in n values was also observed depending upon the choice of exotherm endpoint, but this was not of great magnitude. Therefore, the values of n will be reported and discussed.

Effect of crystallization temperature on the Avrami exponent n. For each of the inherent viscosities listed in *Table 1*, samples were crystallized at several different temperatures following melting at 375°C. In light of the higher melting maximum exhibited by the lowest inherent viscosity sample (scan A in *Figure 2*) a higher melting temperature of 385°C was utilized unless otherwise noted. As mentioned earlier, the range of T_cs covered was not the same for all inherent viscosities. Sample crystallization isotherms for CPI-0.69 in the form of Avrami plots are shown in *Figure 4*. The initial slope of the isotherm corresponds to the Avrami exponent n. The decrease in slope at longer crystallization times shown in *Figure 4*

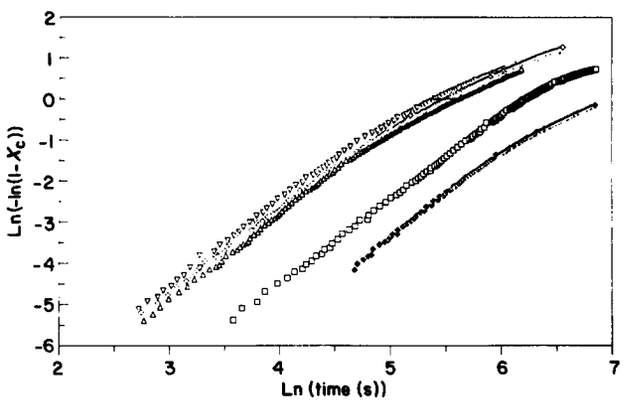

Figure 4 Sample crystallization isotherms for CPI-0.69: Avrami plots as a function of isothermal crystallization temperature: □, 280°C; ▽, 330°C; ◇, 335°C; △, 340°C; +, 345°C

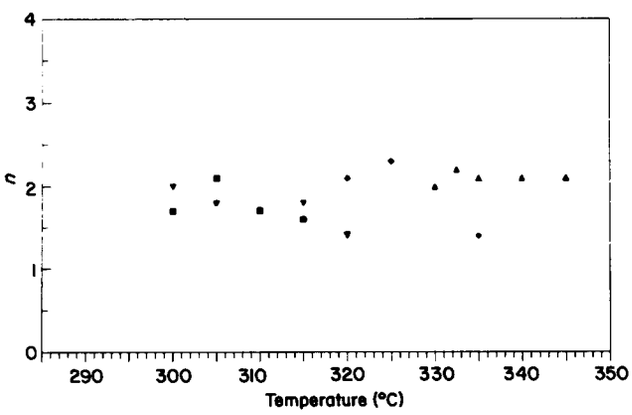

Figure 5 Avrami exponents as a function of isothermal crystallization temperature for LARC-CPI: ■, CPI-1.49; ▼, CPI-1.24; ◆, CPI-1.05; ▲, CPI-0.69

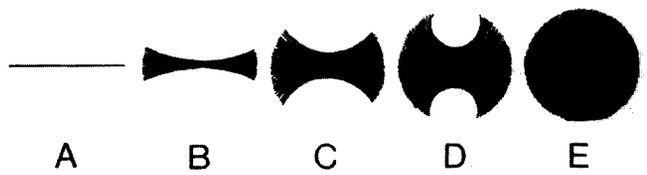

Figure 6 Evolution of spherulitic growth ranging from a folded-chain single crystal (A) to a fully developed spherulite (E)

has been observed for a number of polymers, including other semicrystalline polyimides, poly(ethylene terephthalate) (PET), PEEK and polyethylene[2,40–44]. This lowered exponent value has been attributed to secondary crystallization or changes in crystal perfection[12,44]. A representative plot showing the Avrami exponent as a function of T_c is given in *Figure 5*. The initial part of the slope was used to determine the Avrami exponents shown in the present work. It is important to note that utilization of this initial slope may place some limitations on predictions for the completion of crystallization. In light of the lowered slope observed at longer times, a prediction of crystallization completion based upon the initial slope would be lower than actually occurs. Avrami exponents determined in the higher temperature region of the crystallization window (known as the nucleation-controlled region) are shown whenever possible. This region of the crystallization window is generally more limited with regard to the overall bulk crystalline growth rate because the number of primary nuclei in this temperature range is typically less than for lower temperatures. Returning to *Figure 5*, the Avrami exponents for the different inherent viscosity CPI films are generally close to a value of ~2.0 over the T_c ranges studied. This Avrami exponent value of 2 suggests a sheaf-like (or hedritic) rather than a fully spherulitic morphology often associated with $n=3$ for the case of instantaneous heterogeneous nucleation. *Figure 6* shows a schematic drawing representing the development of a single crystal (A) to a fully developed spherulite (E)[45,46]. The two-dimensional hedritic textures corresponding more to a value of $n=2$ are also depicted (C and D). However, it is important to note that the structure shown in *Figure 6* represents crystalline growth more as a series of two-dimensional plates with little branching. In the event that considerable branching takes place, a more unified three-dimensional structure corresponding more to $n=3$ would be expected.

Referring again to *Figure 5*, several comments may be made with regard to this plot. Generally speaking, the Avrami exponent appears to show little change or a small decrease with increasing T_c. This is surprising, especially for crystallization occurring in the nucleation-controlled region of the crystallization window. With increasing temperature, the nucleation density would be expected to decrease, possibly increasing the dimensionality of growth. It is unclear as to why this apparent small decrease in n is occurring. This trend seems to be consistent for all of the inherent viscosities examined. Another observation from *Figure 5* is that the overall value of the Avrami exponent appears to increase somewhat with decreasing inherent viscosity. A possible explanation may concern the differences in the T_c ranges investigated for the different inherent viscosities; however, no confirmatory arguments based on structural differences can be offered.

Morphology and its dependence on crystallization temperature. Direct observation of morphological features lends credence to the results obtained using crystallization kinetics. The morphology was first investigated using polarized optical microscopy, but no distinguishing features whatsoever were visible by this technique. This was thought to be a consequence of morphological features being either too small, or too nondescript to be observed by this method. Photographic small-angle light scattering (SALS) was next attempted, as it is sometimes possible by this second method to observe structures that are too small to be resolved in the optical microscope[47]. However, while some azimuthally dependent light scattering was observed, again no distinguishing features could be delineated regarding the nature of any superstructure. Electron microscopy was therefore invoked as a means of probing the structure at a finer level.

Electron microscopic studies utilized both SEM combined with a permanganic etching procedure used for revealing fine structure in PEEK, described in an earlier publication[33], and TEM. *Figures 7a* and *b* show the as-cast air and glass surfaces for the lowest inherent viscosity film recrystallized at 280°C. Recalling the Avrami exponent values of ~2 for samples recrystallized at 280°C, the morphological textures observed in the recrystallized as-cast air surface suggest the sheaf-like or hedritic structure affiliated with this value (*Figure 6*).

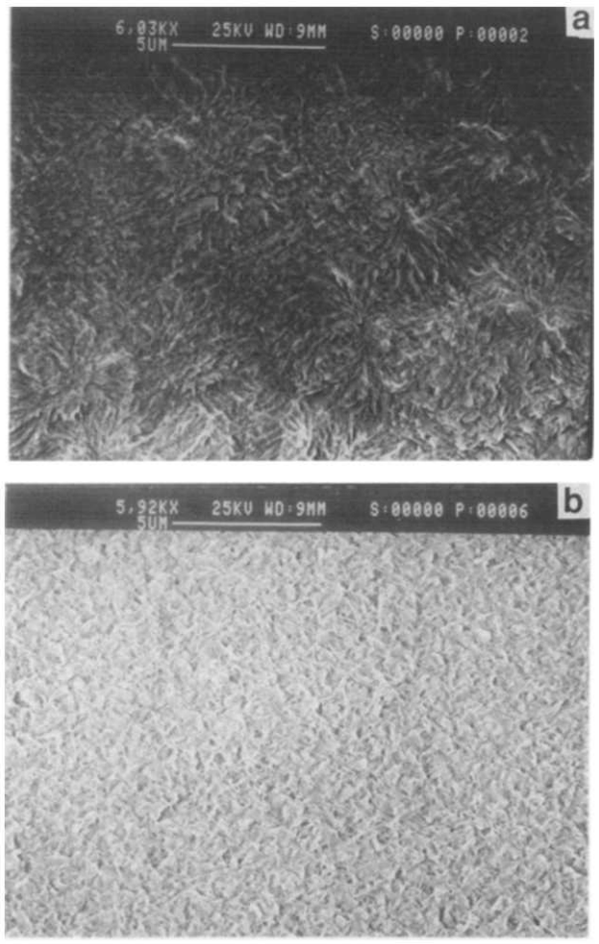

Figure 7 SEM micrographs of permanganate-etched CPI-0.69 recrystallized from the melt at 280°C: (a) as-cast air surface; (b) as-cast glass surface

Noting the size of the superstructure revealed by SEM (~5–10 μm), there is some question as to why no distinguishing features were revealed by either polarized optical microscopy or photographic SALS. One possible explanation involves the polarizability of the chain axis in the radial and tangential directions of the superstructure. If there is an insufficient difference between the two polarizabilities, then no distinct structure would be observed using these two visible light techniques. Sufficient optical anisotropy must exist in the system in order for these features to be visible, which results in birefringence. This possibility is also conceivable in light of a proposed minimized conformation of LARC-CPI using molecular modelling, which will be discussed later. Returning to the SEM results, the consistency of the Avrami exponent with observed structure by SEM as a function of T_c (spanning a range of 55°C) is noteworthy, especially as the temperatures examined here vary from more diffusion-controlled growth to more nucleation-controlled growth nearer to T_m^0 (T_g and T_m^0 are ~220°C and 390°C, respectively). This suggests that the dimensionality of growth for this material appears not to be strongly affected by T_c. The apparent difference in morphologies between the as-cast air and glass surfaces of the films shown in *Figures 7a* and *b* is consistent with observations reported previously[33]. This earlier work showed a similar difference in morphologies between air and glass sides of the as-cast and recrystallized CPI-0.69 film. The issue of apparent morphological differences as a function of casting surface will be readdressed subsequently in light of SEM and TEM data. *Figures 8a* and *b* show CPI-0.69 samples recrystallized at 335°C for several hours which have been etched for 24 and 60 min, respectively. These micrographs consider the effect of etching time on revealed morphology, allowing for the investigation of the bulk structure as well. (Recall that the film thickness is on the order of 25–50 μm.) The results shown in *Figures 8a* and *b* suggest that the hedritic structure revealed on the air side is also representative of that in the bulk of the film, lending more indirect evidence to the Avrami results described earlier. Additional evidence of this morphology in the bulk will be illustrated by TEM results.

The effect of T_c on lamellar texture was also investigated by TEM. Samples of the CPI-0.69 film recrystallized at 280, 300 and 335°C were examined without staining or chemical etching. Results are shown in *Figure 9* for the sample recrystallized at 335°C. As was the case for the as-cast film described in previous work[33], there appears to be a difference in the size of the hedritic superstructure between the two as-cast sides. In all cases, the groups of lamellae appear to form stacks which are sheaf-like in nature. Similarly to the as-cast material, little or no lamellar branching was observed. In view of the hedritic or sheaf-like growth that has been directly observed in these LARC-CPI materials prepared under a variety of conditions, it is believed that the Avrami exponent of ~2 determined by crystallization kinetics might well be expected, since these structures are more two-dimensional in nature. As mentioned previously, the SEM results raise the question as to whether the differences in surface morphologies are actually a structural gradient going from one surface to the other, or surface textural differences. The micrographs shown in *Figures 9a* and *b* were taken at the as-cast air side and the glass side of the film, respectively. Additional micrographs taken in

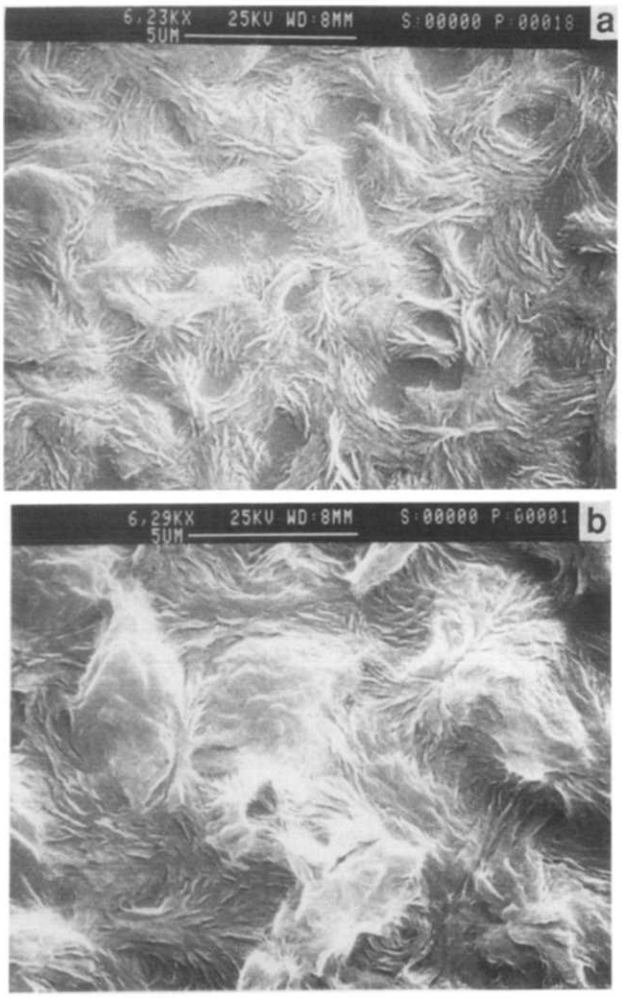

Figure 8 SEM micrographs showing the effect of chemical etching time on observed texture for the as-cast air surface of CPI-0.69 recrystallized from the melt at 335°C. Etching times: (a) 24 min; (b) 60 min

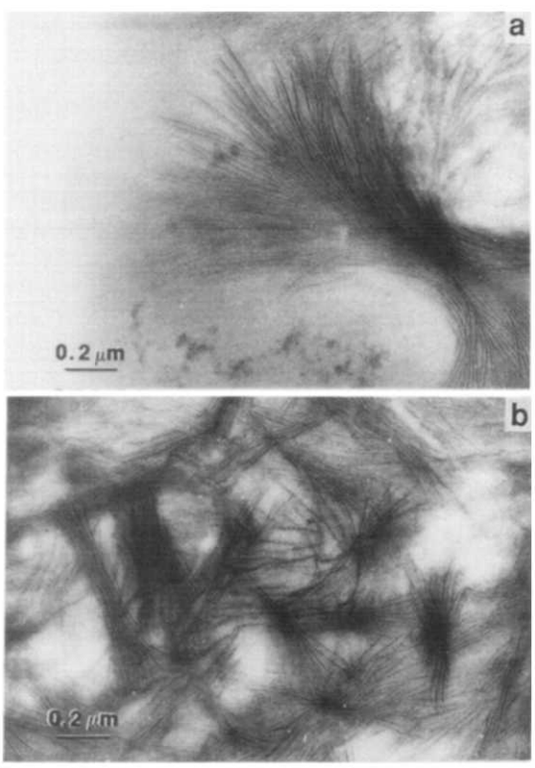

Figure 9 TEM micrographs of untreated CPI-0.69 recrystallized from the melt at 335°C: (a) as-cast air surface; (b) as-cast glass surface

progression through the width of the film from one surface to the other (data not shown) imply that a small gradient in texture very near the glass side may exist, but the structure formed at the air side dominates through most of the film thickness[48]. The sheaf-like stacks appear to be increasing in number and decreasing in size near the glass surface. It is noteworthy that no impurity serving as a nucleation site was large enough to be visible in any of the micrographs. Again, the clarity of microstructure in the LARC-CPI without the use of chemical staining is rather unique.

The effect of ruthenium tetroxide (RuO_4) staining on the contrast of the LARC-CPI samples was also investigated. While the contrast without staining or etching was deemed satisfactory, it was interesting to see whether it would be enhanced by RuO_4. This agent has been shown to be effective in improving the contrast for a number of polymers containing saturated and unsaturated bonds[49]. In the present case, an as-cast air surface of the as-received CPI-0.69 film was monitored as a function of staining time. Surprisingly, there was a loss of structural detail with increasing staining time rather than an enhancement; consequently no data are presented here.

Determination of crystalline growth rate. Based upon the success of SEM in conjunction with permanganic etching to reveal morphological structure, an attempt was made to estimate the isothermal growth rate, G, of the low-inherent-viscosity LARC-CPI designated as CPI-0.69. As mentioned previously, the commonly-utilized techniques of polarized optical microscopy and SALS were not successful when applied to LARC-CPI. Hence, initially amorphous samples were crystallized in the thermal chamber for various short periods of time at a T_c of 335°C and then quenched. The diameters of the hedrites were estimated as a function of time from the SEM micrographs of etched samples. Micrographs showing the growth of the hedrites as a function of time are shown in *Figure 10* for times of 4 and 16 min. A plot showing the resulting linear growth rate estimated for this value of T_c is shown in *Figure 11*. The approximate value of G under these conditions is $0.5\,\mu m\,min^{-1}$. A decrease in the growth rate at longer times would be expected as a result of spherulitic impingement. While the authors recognize that this method yields only an estimate at best, it does at least provide some indication of the linear growth rate value. It is, of course, expected that the growth rate would be a function of both T_c and molecular weight.

Effect of time in the melt on crystallization behaviour. As discussed above, another potential factor influencing the crystallization behaviour of a material is the time spent in the melt. This variable was examined by melting the lowest inherent-viscosity film for different time periods at 385°C. The effect of melt time on the Avrami exponent is shown in *Figure 12*. There is a slight overall decrease in n as a function of melt time. As an increase in melt time would more likely either decrease the number of nuclei, as mentioned earlier due to nuclei destruction, or have little effect, the value of n was anticipated to either increase or remain the same. An assessment of the effect of time in the melt was made using the crystallization exotherm peak temperature upon cooling from the melt, T_{mc}. This value, which is related to overall crystallization,

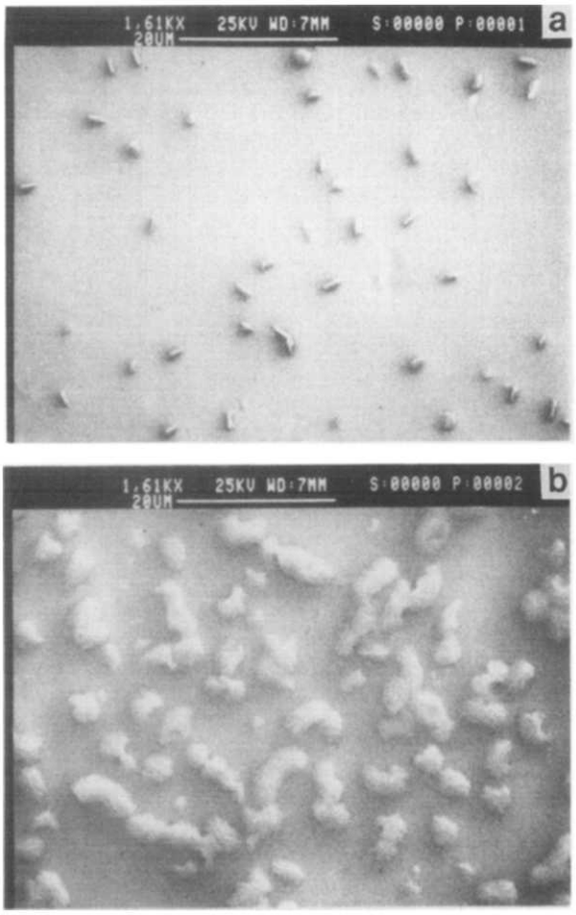

Figure 10 SEM micrographs showing the development of hedrites in CPI-0.69 as a function of crystallization time at $T_c = 335°C$: (a) 4 min; (b) 16 min

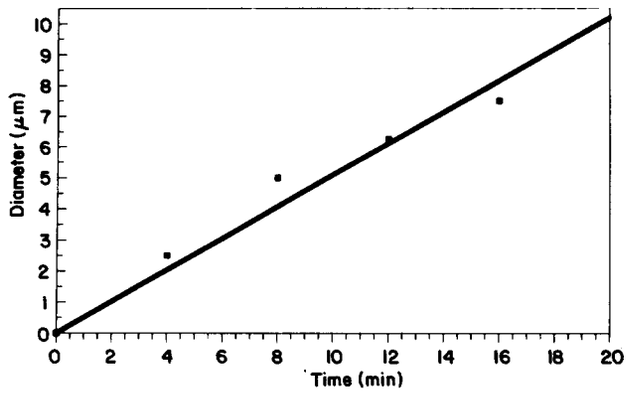

Figure 11 Plot showing diameter of CPI-0.69 hedrites as a function of time at $T_c = 335°C$ used to estimate growth rate G

is influenced by factors such as temperature of the melt, time in the melt, nucleating agents, and molecular weight[25–28]. Samples were melted for various times, then cooled from the melt at a rate of $10°C\,min^{-1}$. Results are shown in *Figure 13*. The decrease in T_{mc} is consistent with the behaviour exhibited by the crystallization exotherms with increasing time in the melt, where the general shape of the overall exotherm as a function of increasing crystallization time shows a widening in breadth and a decrease in intensity. This suggests that crystallization is occurring more slowly with increasing time in the melt, suggesting that the number of nuclei is reduced as a function of melt time.

Effect of melt temperature on crystallization behaviour. As discussed above, another important parameter affecting crystallization behaviour is melt temperature for constant melt time prior to quenching to T_c. Again, the lowest-inherent-viscosity sample was utilized for this study. The melting temperatures investigated were 375, 385 and 395°C.

An initial assessment of the effect of melt temperature was made using d.s.c. by determining T_{mc}. After melting the samples for 2 min at the selected melting temperature, they were cooled at a rate of $10°C\,min^{-1}$ to determine T_{mc}. The resulting d.s.c. scans are shown in *Figure 14*. There is a substantial difference in both T_{mc} and the magnitude of the heat of crystallization when the melting temperature is decreased from 395 to 385°C. As shown in *Figure 14*, T_{mc} increases by over 25°C and the heat of crystallization increases four-fold at the lower value of the melting temperature (385°C). The magnitude of these changes suggests that a substantially larger number of nuclei are destroyed at the higher melt temperature, or a chemical change in the material, such as crosslinking or chain extension, is occurring at this temperature which is responsible for the significant reduction in crystallization. As LARC-CPI is melt-sensitive, there was concern that a chemical change may, in fact, be taking place. This was investigated by isothermally crystallizing samples melted at 395°C from

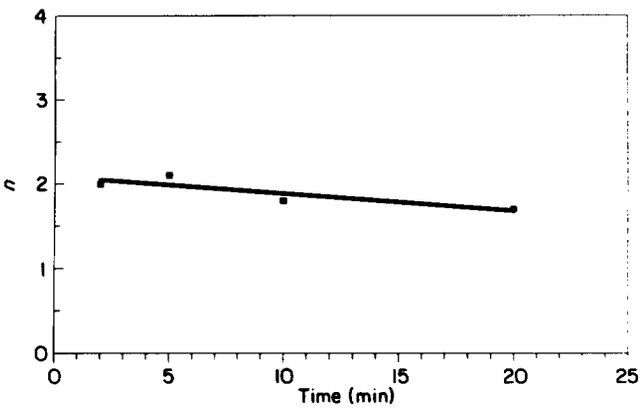

Figure 12 Avrami exponent values for CPI-0.69 crystallized at 330°C as a function of time in the melt at 385°C

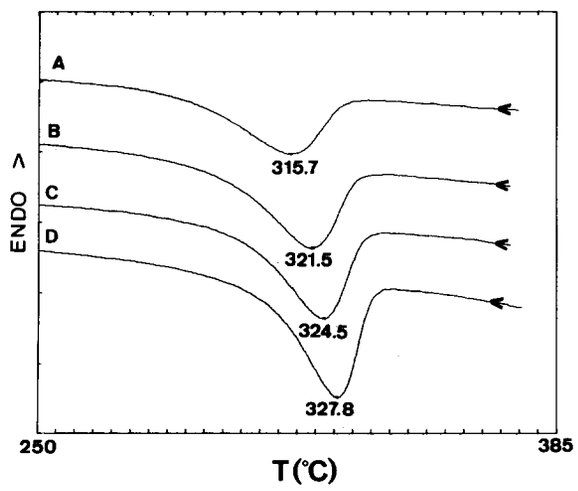

Figure 13 T_{mc} exotherms for CPI-0.69 as a function of time in the melt at 385°C: A, 20 min; B, 10 min; C, 5 min; D, 2 min

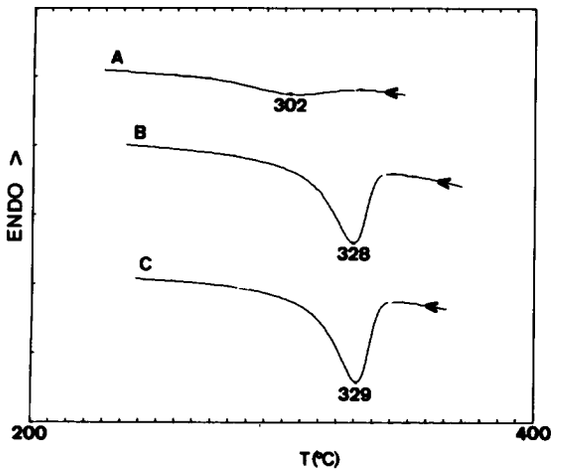

Figure 14 T_{mc} exotherms for CPI-0.69 as a function of melting temperature: A, 395°C; B, 385°C; C, 375°C

the melt, as well as isothermally crystallizing following heating from the glass (after quenching following melting at 395°C). The rationale behind this experiment was that if a chemical change were responsible for the earlier observation, the heat of melting would be about the same whether the sample were crystallized from the melt or glass. On the other hand, if a substantially larger number of nuclei are destroyed but no chemical change is taking place in the melt, the heat of melting would be affected depending upon whether crystallizing from the melt or from the glass at the same T_c. That is, as a consequence of heating from the glass (after rapid quenching) to the same T_c, the nucleation density is generally increased and thus the bulk crystallization rate at T_c is typically higher[50]. Following melting at 395°C, samples were recrystallized at 335°C for ~2 h. The heat of melting value for the sample crystallized from the glass following melting at 395°C was almost twice the value of that quenched from the melt to the same T_c ($\sim 31\,J\,g^{-1}$ *versus* $18\,J\,g^{-1}$). Hence, it is believed that no major chemical change in the material is occurring, or at least not to a substantial degree. Returning to *Figure 14*, differences in T_{mc} and the heat of crystallization do exist such that both values are slightly higher for the sample melted at 375°C. This suggests that the sample melted at the lower temperature has more residual nuclei surviving in the melt, which is in agreement with the conclusions reached by past researchers regarding other crystallizable polymers[2,11,12,39–42].

The effect of melt temperature on the Avrami parameters n and k was also assessed. Samples melted at 385°C crystallized too slowly to generate an exotherm suitable for analysis by our d.s.c. technique. An evaluation was therefore made based on samples melted at 375 and 385°C. Avrami exponents as a function of T_c for these melt temperatures are shown in *Figure 15*. Both sets of values are approximately equal to 2. The trend in n values for samples melted at 375°C could appear to be decreasing slightly with increasing T_c, but the authors believe that the trend in these data is within the data scatter and therefore not significant. For samples melted at 385°C, n appears to be increasing very slightly or remaining the same as a function of T_c. This is more consistent with what was observed by TEM for samples melted at 375 and 385°C.

Evaluation of the equilibrium melting point

The equilibrium melting point is that which represents the 'large' crystal of extended-chain thickness (no significant surface contribution) with the greatest degree of perfection. A common extrapolation procedure used to determine this value is that developed by Hoffman and Weeks[51]. Invoking the model of chain-folded crystallization, this procedure assumes that the size of the fold length of the growing crystal is inversely proportional to the degree of supercooling when undergoing isothermal crystallization. A linear relationship therefore exists between T_c and melting point, T_m. Since the observed T_m increases with increasing T_c at higher T_c values, an extrapolation can be made to the value where $T_m = T_c$ (assuming other variables are constant) which provides the equilibrium melting point T_m^0. Less or no dependence of T_m on T_c is typically observed at lower T_c values due to melting and recrystallization during the heating process[51]. Recalling the TEM data shown previously, a lamellar texture was revealed. Hence, the Hoffman–Weeks method was used to estimate the equilibrium melting point of the lowest inherent viscosity film using $T_m = 385$°C. This lower T_m was utilized as an approximation to a temperature exceeding T_m^0 since the rate of recrystallization was greatly reduced at the higher temperatures investigated. The resulting Hoffman–Weeks plot is shown in *Figure 16*. This plot yields an extrapolated T_m^0 value of 390°C. From this estimate of T_m^0, it is now possible to approximate the actual *versus* an apparent crystallization window for this LARC-CPI, defined as $(T_m^0 - T_g)$. Recalling that the T_g of our CPI

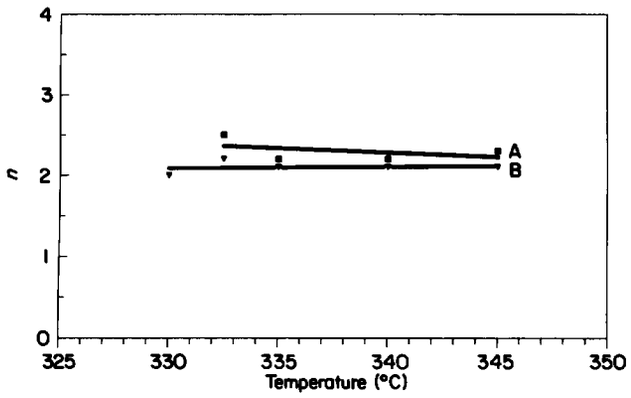

Figure 15 Avrami exponents for CPI-0.69 crystallized at various temperatures as a function of melt temperature: A, 375°C; B, 385°C

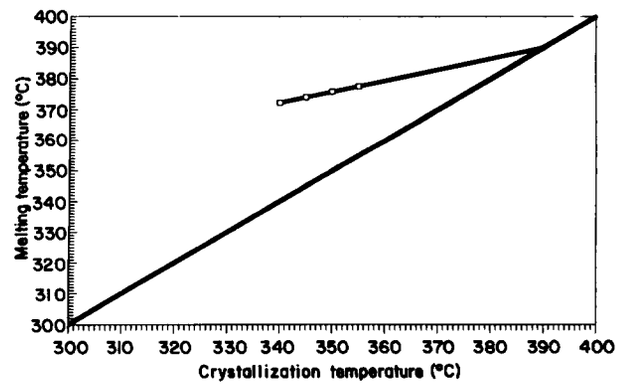

Figure 16 Hoffman–Weeks plot used to estimate the thermodynamic melting point T_m^0 of CPI-0.69

materials is ~220°C, the estimated actual crystallization window is 170°C. This value is lower, for example, than that for PPS, which has an estimated T_m^0 of ~310°C and a T_g of 80°C[52]. Referring again to *Figure 16*, a limited range of T_cs was utilized to determine T_m^0. However, the data do yield a satisfactory correlation coefficient ($R^2=0.996$) so that the extrapolation value for T_m^0 is probably a reasonable estimate. Furthermore, establishing a value of T_m^0 may also shed some light on the crystallization kinetics results. In order to evaluate the true crystallization kinetics behaviour of the 'true melt', it is necessary to melt the material above T_m^0 to erase previous thermal and/or processing history. In the present case, however, recrystallization following melting above 390°C occurred at too slow a rate to enable analysis by our d.s.c. procedure and crystallization kinetics. The results presented here therefore clearly illustrate the influence of previous thermal history. From a practical standpoint, these results imply that regenerating crystallinity in this material in a reasonable time frame following melting may not be possible if the previous crystalline history is erased, i.e. the T_m^0 is surpassed for time-scales on the order of 1 min or more. Our data therefore imply that the crystallization behaviour does significantly depend on the previous thermal (melt) history.

SAXS results

In view of the lamellar morphology revealed by TEM and Hoffman–Weeks extrapolation of T_m^0 for a chain-folded system, further confirmation of fine structure was desired. SAXS was therefore investigated as a means of providing additional evidence. Results for the present work were obtained in the form of a plot of desmeared scattered intensity $I(s)$ as a function of the angular function s; s is defined as $\{2/\lambda\}\sin\theta$, where θ is one-half of the radial scattering angle and λ is the wavelength of the X-ray incident beam. The interlamellar spacing d (or d-spacing) can be approximated by taking the reciprocal of s corresponding to the peak value at the intensity maximum.

Effect of crystallization temperature on SAXS. The effect of T_c on SAXS results was assessed by crystallizing samples of the low-inherent-viscosity film at several temperatures. The desmeared scattering profiles are shown in *Figure 17*. The shoulder in the intensity trace near the incident beam results from the long spacing which is the average centre-to-centre distance of crystalline lamellae with whatever amorphous region exists between them. The qualitative trend shown in *Figure 17* for the long spacing is an increase with increasing T_c. (D.s.c. results suggest little or no increase in the degree of crystallinity as a function of T_c.) As this spacing is evaluated over both crystalline and amorphous regions, this larger value results from an increase in crystalline lamellar thickness with increasing T_c. On the other hand, the broad weak second peak maximum appearing at larger s values ($d=$ ~40–45 Å) did not change, irrespective of T_c and is clearly not the result of a 'second order'. Furthermore, this broad peak completely disappeared from the trace of an amorphous sample, which indicates that its origin is from the crystalline phase. Plots of the long spacing and interdomain or d-spacing values as a function of T_c are shown in *Figure 18*. These values were determined using desmeared data. The long spacing

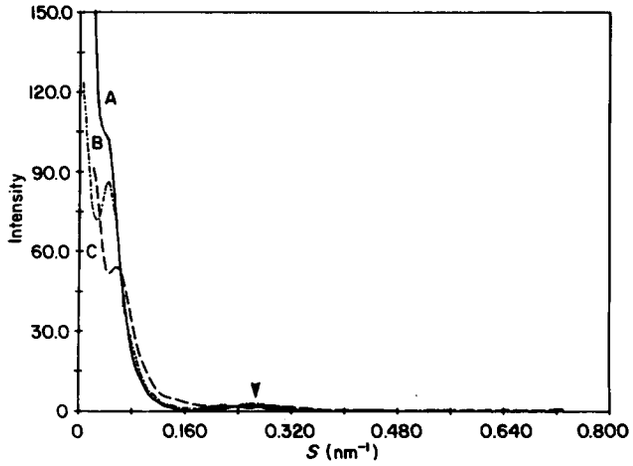

Figure 17 Desmeared SAXS profiles as a function of crystallization temperature from the melt for CPI-0.69: A, 335°C; B, 300°C; C, 280°C

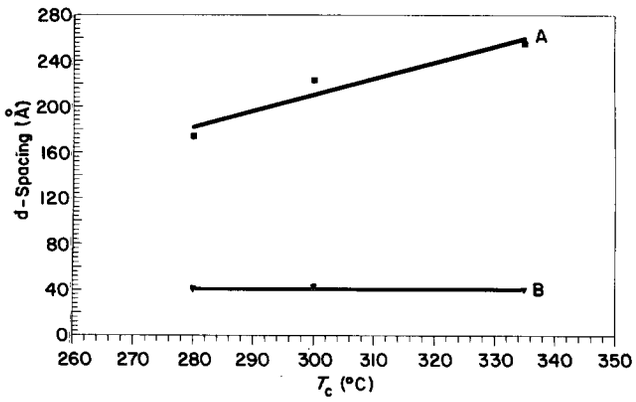

Figure 18 Plots of A, long spacing and B, interdomain spacing values as a function of crystallization temperature for CPI-0.69 using desmeared data

values are larger than the average lamellar thicknesses obtained by TEM, as expected. The fact that the second scattering peak did not change proportionately with the change in the long spacing provides evidence that this second peak is not a higher order reflection affiliated with the long spacing. A hypothesis for the origin of this peak based on molecular modelling will be presented in a later section.

Determination of the heat of fusion for a fully crystalline sample

The heat of melting for a 100% crystalline sample was estimated using a combination of d.s.c. and WAXS. A series of CPI films with different inherent viscosities were crystallized to different levels by varying T_c and time. Differences in levels of crystallinity were first evaluated on a relative basis by measuring heat of melting values using d.s.c. The absolute per cent crystallinity for each film was then determined using WAXS. The series of raw data WAXS curves used for the per cent crystallinity determined is shown in *Figure 19*. Scan A is the scattering curve for the fully amorphous sample and scans B–H correspond to samples in order of increasing crystallinity. The three crystalline peak maxima occur at 2θ values of ~19, 22 and 27° (or d-spacing values of 4.8, 4.0 and 3.3 Å, respectively). These values are consistent with those reported previously by NASA-Langley workers[4–6,34,53–55].

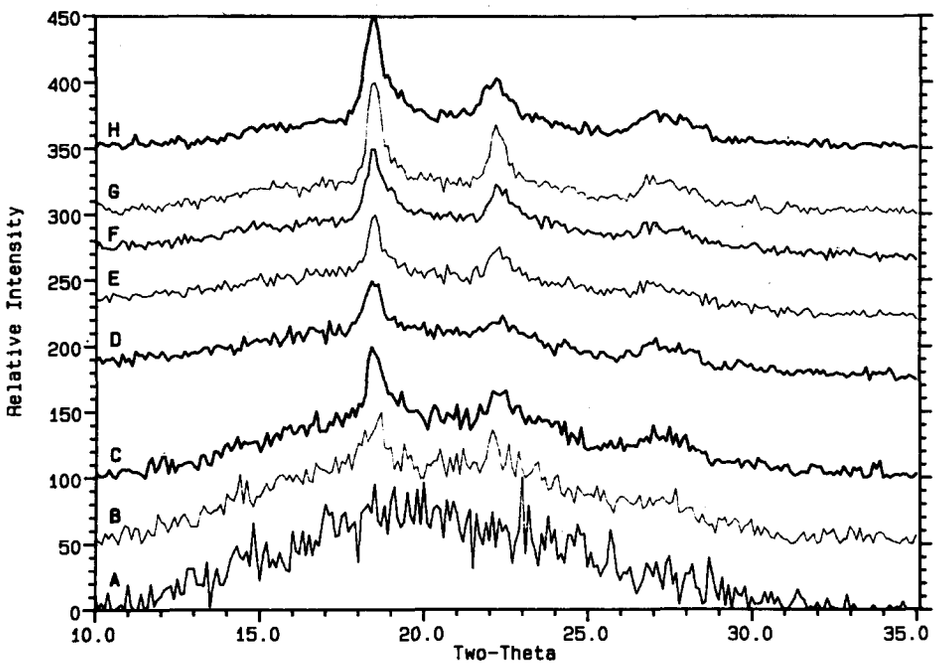

Figure 19 Raw WAXS data used for per cent crystallinity determination: A, amorphous CPI-1.49; B, CPI-1.49: $T_c = 300°C$, $t = 20$ min, quenched from melt; C, CPI-1.49: $T_c = 300°C$, $t = 40$ min; D, CPI-1.49: $T_c = 60$ min; E, CPI = 0.69: $T_c = 335°C$, $t = 4$ min; F, CPI-1.05: $T_c = 330°C$, $t = 60$ min; G, CPI-0.69: $T_c = 335°C$, $t = 36$ h; H, CPI-0.69: as-received

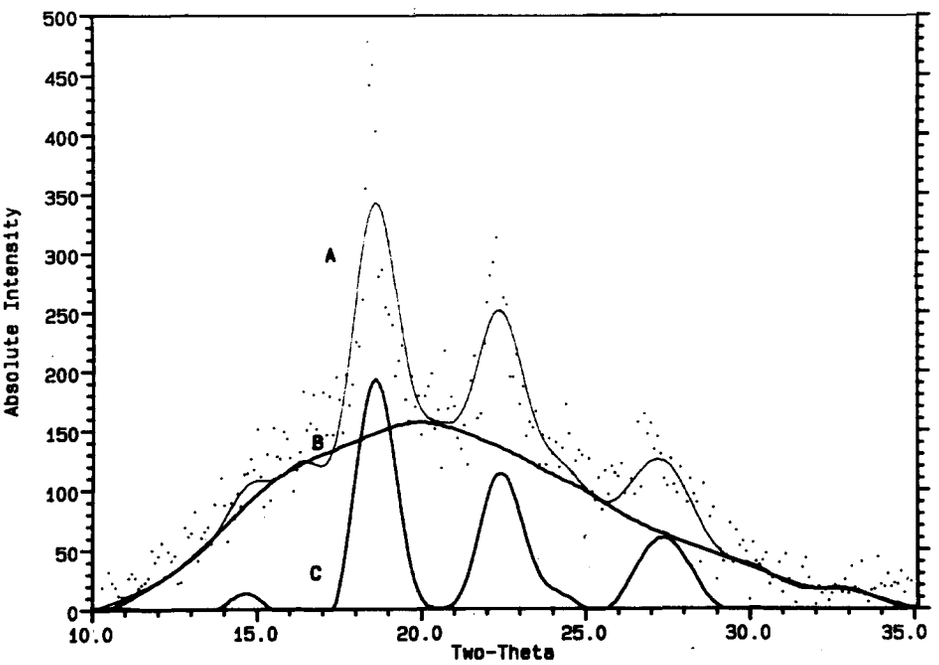

Figure 20 Examples WAXS data illustrating resolution of WAXS data into crystalline and amorphous fractions: A, smoothed raw data; B, amorphous halo used to isolate the crystalline peaks; C, crystalline peaks

Per cent crystallinity was estimated using the general method of peak resolution utilized by Hermans and Weidinger[55–57], and Vonk[58]. This method evaluates crystallinity on an absolute basis by utilizing the ratio of the integrated intensity of the crystalline peak to that of the complete (i.e. crystalline and amorphous components) scans. A potential systematic error may, however, exist in the evaluation of the amorphous halo, resulting in a lower absolute crystallinity value than is actually the case. That is, the method may somewhat overestimate the value of the amorphous intensity because of the likely convolution of thermal diffuse scattering with the amorphous intensity[59]. Thermal diffuse scattering occurs as a consequence of atomic thermal vibrations, and is not easily resolved from the amorphous scattering[60].

In order to separate the crystalline from the amorphous scattering, a fully amorphous sample was scanned to establish the amorphous halo shape. Based upon the assumption that no contributions to the amorphous scattering intensity of the sample occur outside the limits of the halo, it was baseline-corrected using the values where the intensity returned to background level[56]. The data were then smoothed using a Fourier technique as part of the Siemens spectral analysis program to remove high frequency noise. The scans for the semicrystalline samples were baseline-corrected and smoothed analogously to that for the amorphous scan.

An example illustrating crystalline peak resolution is

shown in *Figure 20;* the data points outline the baseline-corrected raw data and curve A is the smoothed scan. Noting the differences in peak intensities between the raw and smoothed data, there may be understandable concern regarding the effect of smoothing on the per cent crystallinity calculation involving integration of the intensity with angle. Comparisons were made using both the raw and smooth data, and results were consistently reproducible to within 2%. It is therefore believed that smoothing does not introduce any serious error into the per cent crystallinity calculation. Curve B shows the amorphous halo used to separate the crystalline peaks from the amorphous scatter. This halo was superimposed on the semicrystalline scattering curve using a series of points connected by a Fourier fitting technique. Again, the shape of the superimposed halo was based upon that for the pure amorphous sample. Following subtraction of the amorphous halo, the resolved crystalline scattering curve was obtained and this is shown by curve C.

A plot was then constructed attempting to correlate heat of fusion values determined by d.s.c. to the per cent crystallinity evaluated by WAXS. This is shown in *Figure 21*. A noteworthy point is that the lowest data point, which appears to be somewhat low in light of the other values, was reverified. As almost all WAXS measurements were conducted using films cast on plate glass, there is a possibility that a systematic error arising from planar biaxial orientation caused by drying stresses or ordered crystalline growth from the surface may exist. However, the data point corresponding to the highest level of crystallinity in *Figure 21* was determined using a powder. Since this final data point is in line with the others obtained utilizing films, it is believed that such an error is not severe, if it exists at all. A linear regression fit of the data ($R^2=0.96$) resulted in an extrapolated heat of fusion value of $\sim 124.6\,\mathrm{J\,g^{-1}}$ for the 100% crystalline sample. This is in reasonable agreement with the value of $\sim 130.5\,\mathrm{J\,g^{-1}}$ reported for another LARC-CPI material prepared elsewhere[61].

Computer modelling of LARC-CPI

As a consequence of the large structural repeat unit of LARC-CPI and evidence by TEM and SAXS for lamellar structure, computer modelling was utilized as a means of gaining insight into the LARC-CPI conformational structure. Several potential conformations were generated and evaluated. The general conformational energy minimization procedure will now be presented.

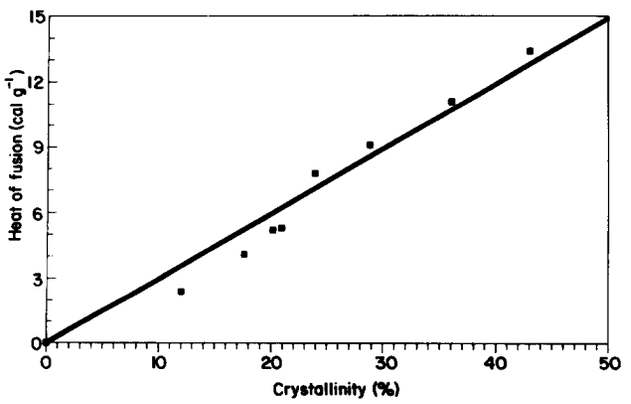

Figure 21 Plot of heat of fusion *versus* per cent crystallinity for LARC-CPI used to determine the heat of fusion for a fully crystalline sample ($1\,\mathrm{cal\,g^{-1}}=4.184\,\mathrm{J\,g^{-1}}$)

Computer modelling procedure for CPI minimum energy conformations. A LARC-CPI repeat unit was first constructed and subjected to repeated cycles of simulated annealing using molecular dynamics. The Tripos force field was employed without electrostatics for all minimization studies reported here. The annealing cycle upper and lower temperatures were 1000 K and 100 K, respectively.

The form of the Tripos force field total conformational energy equation is the sum of the bonded (E_{bonded}) and non-bonded ($E_{\mathrm{non\text{-}bonded}}$) energy terms, defined as:

$$E_{\mathrm{T}}=E_{\mathrm{bonded}}+E_{\mathrm{non\text{-}bonded}} \tag{1}$$

and

$$E_{\mathrm{bonded}}=\sum_{\mathrm{bonds}} E_{\mathrm{bond}}(b_i)+\sum_{\mathrm{angles}} E_{\mathrm{angle}}(\theta_i)+\sum_{\mathrm{tors}} E_{\mathrm{tor}}(\Phi_i)+\sum_{\mathrm{oops}} E_{\mathrm{oop}}(h_i) \tag{2}$$

$$E_{\mathrm{non\text{-}bonded}}=\sum_{i=1}^{n\mathrm{atoms}-1}\sum_{j=i+1}^{n\mathrm{atoms}} E_{\mathrm{nb}}(i,j) \tag{3}$$

where 'tors' denotes all torsional energy terms, 'oops' indicates out-of-plane terms, b_i is the distance between two bonded atoms, θ_i is the angle between three bonded atoms and i is the central atom, h_i is the height of the ith atom above its three neighbouring bonded neighbours (applies to sp^2 carbons and atoms having three neighbours), Φ_i is the torsion angle having central bond i. Four bonded atoms are involved, the two that make up bond i, and the neighbouring atoms on each side of bond i.

Non-bonded energies include electrostatics, van der Waal interactions, and hydrogen bonding. A non-bonded cutoff value of 8 Å, a standard value used in force-field work, was used in the present work. This value is the maximum distance between two atoms i and j for which the energy is to be computed. The energy was neglected for distances exceeding this value[62,63].

Molecules were minimized using the Fletcher–Reeves conjugate gradient algorithm. Details regarding this algorithm are given in the original reference[64]. Minimization was terminated when two successive conformations were within $42\,\mathrm{J\,mol^{-1}}$.

Six representative low-energy conformers from the repeat unit annealing cycle were then chosen for further evaluation. Statistical tests can be performed on a set of molecules to systematically determine whether the set is a fair representation of the conformational variety of the whole. Such a test was not performed for this preliminary study. The six conformers were then subjected to further minimization using the Fletcher–Reeves algorithm mentioned above. The final conformational energies for the six conformers were evaluated using equations (1)–(3). None of the single repeat unit conformers were of sufficient length and regularity to correspond to a truly periodic structure as suggested by the experimental results (see below). The next step was therefore to build structures containing multiple repeat units and search for conformational regularity requiring the fewest number of repeat units.

Each of the resulting minimized conformers was taken as a potential starting point for building a LARC-CPI polymer. A critical assumption was that an actual LARC-CPI polymer is conformationally similar to a model polymer constructed from one or more minimized repeat unit conformers. This assumption is based upon

the further assumption that intermolecular forces are not strong enough to significantly alter the shape of the individual minimized repeat units. Recognizing that this latter assumption may be questionable in light of the polarity of the molecule, this was taken as the simplest hypothesis for building a periodic structure based on the available data.

Oligomers consisting of five repeat units were then constructed from each of the conformers and were energy-minimized. In each case, the central repeat unit was extracted to be used to build larger polymers. The purpose of this step was to create a repeat unit in each case that was close to the original minimum but also took into account some of the slight conformational shifts resulting from a repeat unit being placed in a 'polymer chain environment'. Polymers consisting of 50 repeat units were constructed from each of the extracted central oligomer units and rigorously minimized. Rigorous minimization resulted in termination when the successive conformations were within $4.2\,\mathrm{J\,mol^{-1}}$ rather than $42\,\mathrm{J\,mol^{-1}}$.

LARC-CPI computer modelling results. Repeat unit conformers. The overall shape was similar for five of the six repeat unit conformers and was extended or 'straight'. The shape of the remaining conformer was 'curved'. The end-to-end distance of the latter repeat unit was ~ 11 Å. The conformation energies for the six conformers were also evaluated following final minimization. The 'curved' repeat unit conformer was lowest in energy by a modest amount of $\sim 4200\,\mathrm{J\,mol^{-1}}$. This lowest energy 'curved' conformer is shown in *Figure 22*.

Polymer conformers. Based upon the modest energy differences between conformers, constructing a polymer using a single unit to represent the actual polymer conformation must be regarded as an assumption. Here, this 'build-up' procedure represents the simplest hypothesis from which suitable conformers could be derived. No attempt was made to prove that any polymer conformation generated represents a global energy minimum. If one of the conformers were significantly lower in energy compared to the others, then this representation would most likely be valid.

An attempt was made to define an approximately constant periodic repeat distance between corresponding atoms located at a distance of one or more CPI structural repeat unit(s) apart. Of the six polymers constructed, the

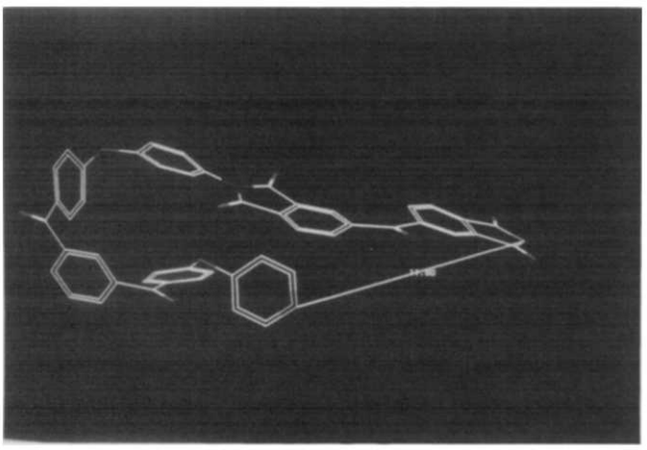

Figure 22 LARC-CPI 'curved' repeat unit of minimal conformational energy. The end-to-end distance is ~ 12 Å

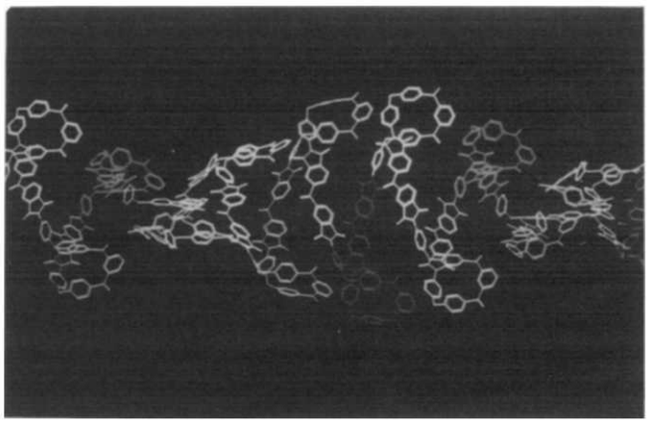

Figure 23 Minimized helical structure of LARC-CPI polymer with a near-periodic repeat distance of 45 Å. Approximately 9–10 structural repeat units are contained in one helical turn

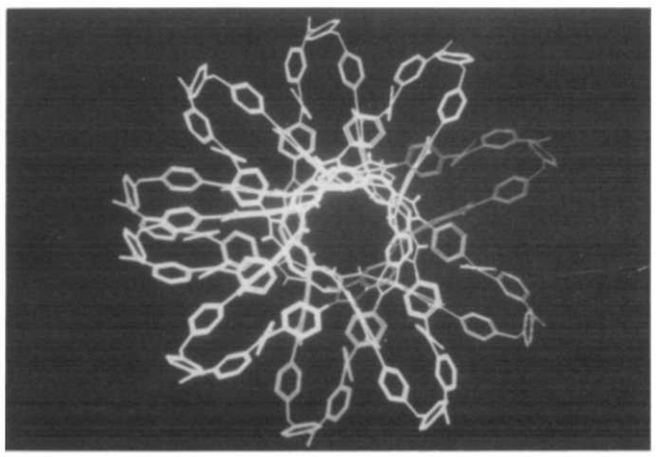

Figure 24 Axial view of the minimized conformational model of LARC-CPI shown in *Figure 22*

five based upon the 'straight' repeat unit conformers did not show any such periodicity. The polymer derived from the 'curved' conformer revealed an unusual helical structure having a near-periodic repeat distance along the chain axis of approximately 45 Å. This helical conformation is shown in *Figure 23*, and an axial view of the conformation is shown in *Figure 24*. Referring to *Figure 23*, each helix contains 9–10 chemical structural repeat units. *Figure 24* shows that there is a helical twist angle of about 35–40° per turn or approximately two repeat units as the helix progresses. Again, this corresponds to between 9 and 10 structural repeat units per repeat of the helical unit along the chain axis. As each repeat unit has a molecular weight of 787, this corresponds to an approximate helical repeat molecular weight of $7870\,\mathrm{g\,mol^{-1}}$. The structural regularity in both directions shown in *Figures 23* and *24* implies that the polymer constructed from this 'curved' repeat unit conformer could be a reasonable possibility for representing the actual polymer.

Comparison of LARC-CPI computer modelling results to SAXS results. An extremely interesting independent feature to evolve from the molecular modelling results is the helical repeat distance of ~ 45 Å. Recalling the earlier TEM results, the average lamellar thickness of the various CPI samples subjected to different thermal conditions was on the order of 100 Å. The periodicity of twist of the

minimized structure, should it be an accurate prediction, could provide only 2–3 helical repeats per lamellar thickness. As a consequence, considerable breadth would be given to the associated interference peak by SAXS corresponding to this periodicity[65]. Recalling the earlier SAXS results, a second, weak, broad interference peak consistently appeared in the range of 40–45 Å for only semicrystalline CPI films, irrespective of inherent viscosity or crystallization conditions. It is realized that the apparent matching of the modelling results with the SAXS data is not in itself proof of the proposed helical conformation. Additional information, such as determining the LARC-CPI crystal unit cell structure, would be necessary to establish the validity of this hypothesized helical conformation. As yet, this has not been established. The density of the proposed conformation was determined by manually docking several polymer chains. This procedure gave a crystalline density slightly above $0.4\,g\,cm^{-3}$. This extraordinarily low density suggests that the LARC-CPI conformation consistent with available SAXS data may remain to be found.

In summary, the modelling study presented above has shown that the SAXS interference peak between 40 and 45 Å is inconsistent with a single repeat unit periodicity in the LARC-CPI chain. By generating a polymer that is consistent with the lowest energy monomer, a LARC-CPI conformer can be hypothesized that is consistent with the SAXS data, but whose unusual projected properties require further examination.

Effect of nucleating agents on the recrystallizability of LARC-CPI

Nucleating agents have been utilized as one means for increasing the crystallizability of a material through increasing the nucleation density. Recalling *Table 1*, it was mentioned that the two CPIs having the highest precursor poly(amic acid) inherent viscosities did not readily recrystallize when heated following melting and quenching. A study was therefore conducted to evaluate the effect of several potential nucleating agents on one of these CPIs with the highest inherent viscosity values.

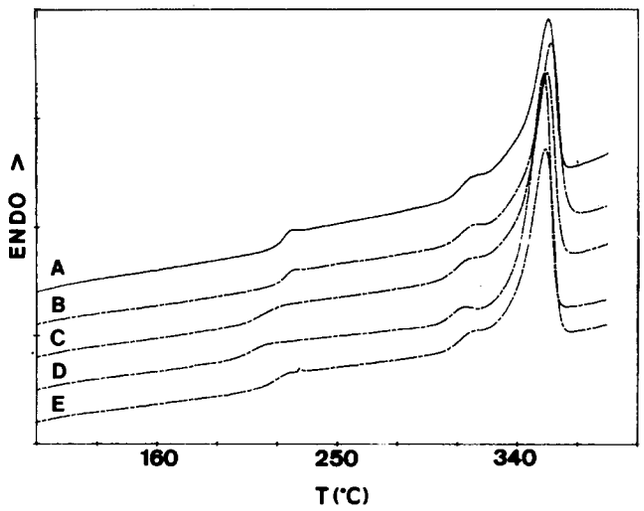

Figure 25 Initial d.s.c. scans of as-cast LARC-CPI as a function of nucleating agent: A, FC-CPI-1.24; B, FC-CPI-1.24 (CPI-0.40); C, FC-CPI-1.24 (PDA-PA); D, FC-CPI-1.24 (3,4′ DABP-PA); E, FC-CPI-1.24 (4,4′ DABP-PA)

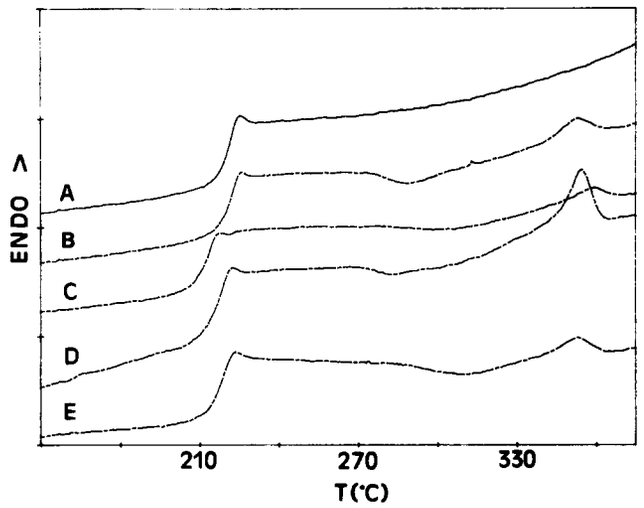

Figure 26 Second d.s.c. scans of as-cast LARC-CPI following an initial scan and quench: A, FC-CPI-1.24; B, FC-CPI-1.24 (CPI-0.40); C, FC-CPI-1.24 (PDA-PA); D, FC-CPI-1.24 (3,4′ DABP-PA); E, FC-CPI-1.24 (4,4′ DABP-PA)

Evaluation of nucleating agents. D.s.c. scans for the as-cast films containing the respective agents described in the Experimental section (also recall *Table 2*) are shown in *Figure 25*. (Nomenclature used in *Figures 25–29* is as described in the Experimental section.) No evidence of two melting peaks was observed for any of the nucleated films; this would have indicated phase separation of the agent from the matrix. All films had an initial melting point approximately equal to that of the control film. There is a small endotherm appearing in the range 310–320°C, similar to that observed for the as-received films from NASA-Langley. Again, this is a consequence of melting of small imperfect crystals formed during the third imidization stage at 300°C. The T_g was somewhat depressed for the films nucleated with the three low-molecular-weight nucleating agents, especially for that nucleated with 3,4′ DABP-PA. The T_g depression of the LARC-CPI films nucleated with the low-molecular-weight agents ranged from ~5 to 10°C. This may well be a consequence of using a high per cent loading of nucleator (as commercial levels are typically in the range of fractional to 1%). Additionally, no separate melting or crystallization peak was observed for any of the low-molecular-weight agents once added to the LARC-CPI, and the T_gs of the nucleated materials were slightly depressed. Thus, these nucleating agents have a small plasticization effect on the LARC-CPI. Another point is that if the nucleator were molecularly dispersed then the T_g could be affected, but if the nucleating agent crystallized as a separate phase, then the T_g would clearly not be affected.

The effect of the nucleating agents was first assessed by d.s.c. Samples were heated to 375°C, quenched and rescanned to test whether the nucleating agents enhanced crystallinity at a rate rapid enough to be detected during the actual scan. Results are shown in *Figure 26* for the four nucleated and unnucleated control films. Referring to *Figure 26*, the control film showed no detectable crystallinity when scanned the second time. Evidence of a crystallization exotherm is apparent in scans B–E, corresponding to the four nucleated films. This is especially observable in scans B and D, corresponding to the films containing PDA-PA and 3,4′ DABP-PA

nucleating agents, respectively. All four nucleating agents induced some slight level of detectable crystallinity, but the 3,4′ DABP-PA nucleator induced more crystallinity under these conditions. The average heat of melting value was four times higher ($\sim 3.3\,\mathrm{J\,g^{-1}}$) than for the others. This result was somewhat surprising, as the two most promising nucleating agents (on the basis of T_m) were the low-inherent-viscosity CPI powder and the PDA-PA. The lower level of crystallinity in the films nucleated by these agents may be related to the fact that neither of these materials dissolved in DMAc at room temperature. As a consequence, the nucleating agent was not so well dispersed throughout the poly(amic acid) solution, which may have limited its effectiveness. Since the 3,4′ DABP-PA nucleated film clearly showed greater recrystallizability relative to the other films, which were essentially equivalent, this film was chosen for further evaluation.

The effect of 3,4′ DABP-PA was further investigated by d.s.c. Samples were melted, then cooled at a rate of $10°\mathrm{C\,min^{-1}}$ to measure T_{mc}. As mentioned earlier, T_{mc} is affected by factors including nucleating agents. Khanna and Reimschuessel, for example, reported an increase of 7°C in the T_{mc} of nylon-6 following the addition of a nucleating agent[25–28]. The effect of 3,4 DABP-PA on the T_{mc} of the CPI is shown in *Figure 27*. The control film (containing no nucleating agent) showed no detectable T_{mc}, whereas the 3,4′ DABP-PA showed a T_{mc} of 309°C.

Effect of nucleating agent on morphology of LARC-CPI. The effect of 3,4′ DABP-PA on the morphology of the LARC-CPI film was investigated using electron microscopy. Two types of films were examined: the as-cast, and the melted and recrystallized[48]. As the effect of the nucleating agent on morphology is even more prevalent for film which has been melted and isothermally recrystallized, these results will be shown here. The films were thermally treated using the thermal chambers described previously[33]. In the present case, they were crystallized for 0.5 h at 300°C following melting at 375°C for several minutes. Samples were examined by both SEM and TEM, using the preparations and procedures described earlier[48]. While both techniques showed differences in morphologies as a function of nucleating agent,

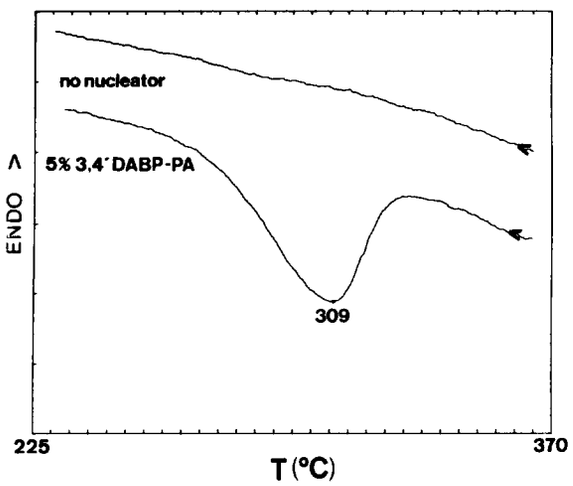

Figure 27 T_{mc} exotherms for as-cast CPI-1.24 as a function of nucleating agent

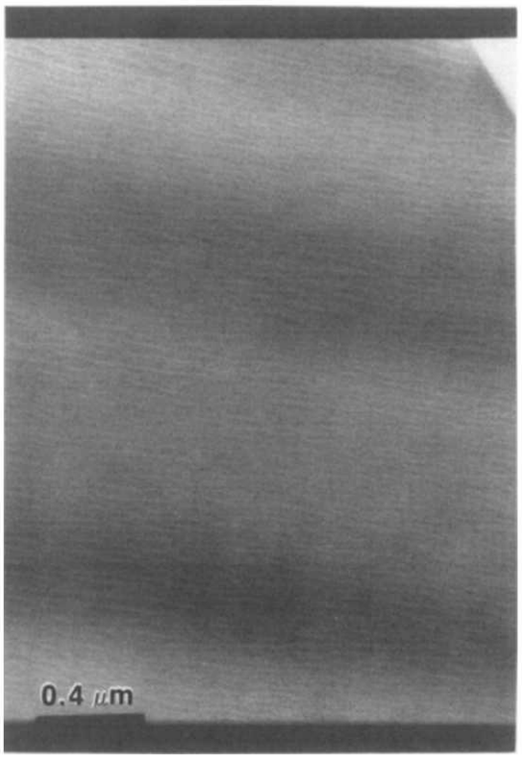

Figure 28 TEM micrograph of untreated FC-CPI-1.24 recrystallized from the melt at 300°C

Figure 29 TEM micrograph of untreated FC-CPI-1.24 (3,4′ DABP-PA) recrystallized from the melt at 300°C

the TEM results are most revealing and will therefore be presented here.

Example TEM micrographs of the recrystallized unnucleated and nucleated films are shown in *Figures 28* and *29*, respectively. As was the case for *Figure 9*, no chemical stains or etchants were employed in conjunction with TEM. It is obvious that significant differences exist

between the morphologies of the two films. The unnucleated film shown in *Figure 28* does not appear to have any distinctive morphology. On the other hand, the texture in *Figure 29* is clearly reminiscent of that observed for the recrystallized lowest inherent viscosity film shown in *Figure 9*. The pronounced morphological differences between the recrystallized films suggest that the effect of the nucleating agent is more pronounced during recrystallization *versus* the original imidization process, as was expected based upon the earlier d.s.c. observations.

SUMMARY

The crystallization behaviour of LARC-CPI was considered as a function of inherent viscosity, crystallization temperature, melting temperature and time in the melt, using several characterization techniques. Assuming heterogeneous nucleation, the Avrami exponent n was consistently in the range of 2, suggesting sheaf-like or hedritic structure. SEM in conjunction with permanganic etching revealed a difference in morphology between the two as-cast surfaces of the film. Furthermore, a sheaf-like texture corresponding to the Avrami exponent of about 2 was revealed irrespective of crystallization temperature. The growth rate of the lowest inherent viscosity film used in this study recrystallized at 335°C was approximated to be $0.5\,\mu m\,min^{-1}$ by use of SEM procedures. TEM results lent support to the differences in morphology as a function of casting surface and the hedritic texture observed using etching and SEM. Thicknesses of lamellae forming sheaf-like stacks were on the order of 100 Å near both film surfaces. SAXS yielded long spacing values which were larger than lamellar thicknesses determined by TEM, as expected. These values increased as a function of increasing crystallization temperature, also as expected. A second low broad SAXS peak with a maximum at ~45 Å was also observed, irrespective of thermal treatment or inherent viscosity, for all semicrystalline films investigated. The heat of fusion for a fully-crystalline LARC-CPI sample was estimated to be $125\,J\,g^{-1}$ using the combined techniques of d.s.c. and WAXS. Conformational investigations of LARC-CPI using computer modelling led to a predicted conformation helical in nature and having a near-periodic repeat distance of 45 Å. While not conclusive, this model is offered as a hypothesis for the presence of the second SAXS peak. The effect of several potential nucleating agents on the recrystallization of a higher inherent viscosity LARC-CPI was assessed by d.s.c., SEM and TEM. Of the four nucleators investigated, including a very low inherent viscosity LARC-CPI and three low molecular weight compounds, phthalic anhydride end-capped 3,4′ DABP-PA was determined to be the most promising.

ACKNOWLEDGEMENTS

The authors gratefully acknowledge Mr D. K. Brandom and Mr S. R. McCartney at Virginia Tech for assistance with Avrami analysis software and TEM sample preparation and operation respectively, as well as Dr S. J. Havens, Mr P. M. Hergenrother and Dr T. L. St Clair, at NASA-Langley for supplying the LARC-CPI and low-molecular-weight materials and for helpful discussions, and Ms C. R. Gautreaux at NASA-Langley and Ms M. K. Gerber at Procter and Gamble for helpful discussions. Financial support provided by the Virginia Institute for Material Systems at Virginia Tech, NASA-Langley Research Center, and the NSF Science and Technology Center: High Performance Polymeric Adhesives and Composites at Virginia Tech is also greatly appreciated.

REFERENCES

1 Verbicky, J. W. in 'Encyclopedia of Polymer Science and Engineering', (Eds H. F. Mark *et al.*), 2nd edn, Vol. 12, Wiley and Sons, New York, 1988, p. 364
2 Cheng, S. Z. D., Herberer, D. P., Lien, H.-S. and Harris, F. W. *J. Polym. Sci., Polym. Phys. Edn* 1990, **28**, 655
3 Takahashi, N., Yoon, D. Y. and Parrish, W. *Macromolecules* 1984, **17**, 2583
4 Hergenrother, P. M., Wakelyn, N. T. and Havens, S. J. *J. Polym. Sci., Polym. Chem. Edn* 1987, **25**, 1093
5 Hergenrother, P. M. and Havens, S. J. *J. Polym. Sci., Polym. Chem. Edn* 1989, **27**, 1161
6 Hergenrother, P. M. and Havens, S. J. *SAMPE J.* 1988, **24**(4), 13
7 Takekoshi, T. in 'Advances in Polymer Science 94: New Polymeric Materials', Springer-Verlag, Berlin, 1990, p. 1
8 Bureau, J.-M., Bernard, F. and Broussoux, D. *Rev. Tech. Thomson-CSF* 1989, **20–21**, 689
9 Heberer, D. P., Cheng, S. D. Z., Barley, J. S., Lien, S. H.-S., Bryant, R. G. and Harris, F. W. *Macromolecules* 1991, **24**, 1890
10 Cheng, S. D. Z., Heberer, D. P., Janimak, J. J., Lien, S. H.-S. and Harris, F. W. *Polymer* 1991, **32**, 2053
11 Day, M., Suprunchuk, T., Deslandes, Y. and Wiles, D. M. *Proc. 34th Int. SAMPE Symp. Exhib.* 8–11 May 1989
12 Wunderlich, B. 'Macromolecular Physics, Volume 2: Crystal Nucleation, Growth, and Annealing', Academic Press, New York, 1976
13 Cebe, P., Hong, S.-D., Chung, S. and Gupta, A. Special Technical Publication 937, American Society of Testing and Materials, Philadelphia, 1987, p. 342
14 Carpenter, J. *SAMPE J.* 1988, **24**, 36
15 Lee, Y. and Porter, R. S. *Macromolecules* 1988, **21**, 2770
16 Bassett, D. C., Olley, R. H. and Al Raheil, I. A. M. *Polymer* 1988, **29**, 1745
17 Blundell, D. J., Chalmers, J. M., Mackenzie, M. W. and Gaskin, W. F. *SAMPE Q.* 1985, **16**, 22
18 Talbott, M. F., Springer, G. S. and Berglund, L. A. *J. Comp. Mater.* 1987, **21**, 1056
19 Lee, Y. and Porter, R. S. *Polym. Eng. Sci.* 1986, **26**, 633
20 Velisaris, C. and Sefaris, J. C. *Polym. Eng. Sci.* 1986, **26**, 1573
21 Lee, W. J., Fukai, B. K., Seferis, J. C. and Cheng, I. Y. *Composites* 1988, **19**, 473
22 Kelly, J. E. and Baird, D. G. *Proc. 36th Int. SAMPE Exhib.* 1991, 1535
23 Pipes, R. B., Brady, D. G., Gibbs, H., Hartness, T., Kardos, J., Litt, M. H., Matsuoko, H., Quinlivan, J. P. and Wilkins, D. Report of the Committee on Thermoplastic Composites in Structural Components, National Materials Advisory Board, National Research Council, NMAB-434, National Academy Press, Alexandria, VA, 1987
24 Chu, J.-N. and Schultz, J. M. *J. Mater. Sci.* 1990, **25**, 3746
25 Khanna, Y. P. and Reimschuessel, A. C. *J. Appl. Polym. Sci.* 1988, **35**, 2259
26 Khanna, Y. P., Reimschuessel, A. C., Banjerjie, A. and Altman, C. *Polym. Eng. Sci.* 1988, **28**, 1600
27 Khanna, Y. P., Kumar, R. and Reimschuessel, A. C. *Polym. Eng. Sci.* 1988, **28**, 1607
28 Khanna, Y. P., Kumar, R. and Reimschuessel, A. C. *Polym. Eng. Sci.* 1988, **28**, 1612
29 Van Antwerpen, F. and van Krevelen, D. W. *J. Polym. Sci., Polym. Phys. Edn* 1972, **10**, 2423
30 Thierry, A., Straupé, C. and Wittman, J. C. *Polym. Commun.* 1990, **31**, 299
31 Groeninckx, G., Berghmans, H., Overbergh, N. and Smets, G. *J. Polym. Sci., Polym. Phys. Edn* 1974, **12**, 303
32 Hergenrother, P. M. in 'Polyimides' (Eds. R. Wilson, H. D. Stenzenberger, and P. M. Hergenrother), Blackie, Glasgow, 1990, p. 158
33 Muellerleile, J. T., Wilkes, G. L. and York, G. A. *Polym. Commun.* 1991, **32**, 176
34 Hergenrother, P. M., Beltz, M. W. and Havens, S. J. *Proc. 34th*

Int. SAMPE Symp. Exhib. 1989, **34**, 963
35 Muellerleile, J. T. and Wilkes, G. L. *Polym. Prepr.* 1990, **31**, 637
36 Olley, R. H., Bassett, D. C. and Blundell, D. J. *Polymer* 1986, **27**, 344
37 Vonk, C. G. *J. Appl. Crystallogr.* 1971, **4**, 340
38 Havens, S. J. personal communications, 1990, 1991
39 Magill, J. H. *J. Appl. Phys.* 1964, **35**, 3249
40 Vilanova, P. C., Ribas, S. M. and Guzman, G. M. *Polymer* 1985, **26**, 423
41 Mingbi, Q., Xiaonan, X., Jun, Z., Wei, W. and Zongneng, Q. *Thermochim. Acta* 1988, **134**, 223
42 Peterlin, A. *J. Appl. Phys.* 1964, **35**, 75
43 Ergoz, E., Fatou, J. G. and Mandelkern, L. *Macromolecules* 1972, **5**, 147
44 Perez-Cardenas, F. C., del Castillo, L. F. and Vera-Graziano, R. *J. Appl. Polym. Sci.* 1991, **43**, 779
45 Khoury, F. and Passaglia, E. in 'Treatise in Solid-State Chemistry, Vol. 3', (Ed. N. B. Hanney), Plenum Press, New York, 1976, p. 335
46 Cheng, S. Z., Barley, J. S. and Giusti, P. A. *Polymer* 1990, **31**, 845
47 Wilkes, G. L. in 'Encyclopedia of Polymer Science and Engineering', 2nd edn), Vol. 14 (Eds H. F. Mark *et al.*), John Wiley and Sons, New York, 1988, p. 542
48 Muellerleile, J. T. PhD Dissertation, Virginia Polytechnic Institute and State University, 1991
49 Polysciences, Inc., Ruthenium Tetroxide 0.5% Aqueous Solution Data Sheet no. 320, 1990
50 Van Krevelen, D. W. *Chimia* 1978, **32**, 279
51 Hoffman, J. D. and Weeks, J. J. *J. Res. Natl Bur. Stand.-A. Phys. Chem.* 1962, **66A**, 13
52 Lopez, L. C. and Wilkes, G. L. *Polymer* 1988, **29**, 106
53 Hergenrother, P. M. and Havens, S. J. *Proc. 36th Int. SAMPE Symp. Exhib.* 1989, **34**, 963
54 Hergenrother, P. M. and Havens, S. J. in 'Polyimides: Materials, Chemistry, and Characterization' (Eds C. Feger, M. M. Khojasteh and J. E. McGrath), Elsevier Science Publishers, Amsterdam, 1989, p. 453
55 Hermans, P. H. and Weidinger, A. *Text. Res. J.* 1961, **31**, 558
56 Alexander, L. E. 'X-Ray Diffraction Methods in Polymer Science', Robert E. Krieger Publishing Co., Malabar, 1985
57 Hindeleh, A. M. and Johnson, D. J. *Polymer* 1978, **19**, 27
58 Vonk, C. G. *J. Appl. Crystallogr.* 1973, **6**, 148
59 Janzen, J. personal communication, 1991
60 Ruland, W. *Acta Crystallogr.* 1961, **14**, 1180
61 Foster-Miller, Inc., personal communication to NASA-Langley Research Center, 1990
62 Clark, M., Cramer III, R. D. and van Opdenbosch, N. *J. Comp. Chem.* 1989, **10**, 982
63 Simeroth, P. E., 'Tripos Force-Field Summary', internal document of Tripos Associates, Inc., St. Louis, 1991
64 Fletcher, R. and Reeves, C. M. *Comp. J.* 1965, **7**, 149
65 Kakudo, M. and Kasai, N. 'X-Ray Diffraction by Polymers', Kodansha Ltd, Tokyo, 1972